Nanophotonics with Plasmonic Nanorod Metamaterials

Diane J. Roth,* Alexey V. Krasavin, and Anatoly V. Zayats*

Taking advantage of their unique and tuneable electromagnetic properties, plasmonic metamaterials constitute a versatile platform for a variety of applications ranging from high-resolution imaging, sensing and spontaneous emission engineering to ultrafast nonlinear optics and light polarization control. Here, recent advances in the design and applications of plasmonic metamaterials based on aligned metallic nanorod assemblies are reviewed, and the fast-developing trends in their exploitation in nanophotonics are outlined. The fabrication of the nanorod-based metamaterials is introduced and their linear and nonlinear optical properties are presented from both microscopic and phenomenological considerations. Multiscale structuring allowing precise engineering of the electromagnetic modes supported by the nanorod metamaterials, as well as nonlocal spatial dispersion effects and their impact on nanophotonic performance are discussed. To illustrate the developing field of practical applications of these metamaterials, some of their main application domains in sensing, photochemistry and nonlinear optics are overviewed and novel designs of anisotropic metamaterials directly derived from the nanorod architecture are introduced.

1. Introduction

Optical metamaterials are commonly defined as nanostructured materials with engineered enhanced electromagnetic properties often going beyond those found in nature. They are typically composed of subwavelength building blocks, or meta-atoms and, similarly to how the properties of conventional materials at the macroscopic scale are defined by the assemblies of atoms they consist of, the electromagnetic properties of metamaterials arise from the material properties of the meta-atoms, their spatial arrangement and the optical interaction between them. Milestones in the development of metamaterials include theoretical and experimental demonstrations of negative-index materials,[1–3] the design of super- and hyper-lenses for diffraction-unlimited high-resolution imaging, cloaking and perfect absorption effects.[4–8]

D. J. Roth, A. V. Krasavin, A. V. Zayats
Department of Physics and London Centre for Nanotechnology
King's College London
Strand WC2R 2LS, London, United Kingdom
E-mail: diane.roth@kcl.ac.uk; a.zayats@kcl.ac.uk

Applications of metamaterials are now realized over a broad frequency range, from microwaves all the way to optical frequencies,[9–12] taking advantage of new fabrication techniques available to achieve the required sizes of meta-atoms and spacing between them. In the UV/vis and NIR spectral ranges, metamaterials can be made of a combination of dielectric materials and metallic structures supporting surface plasmon excitations, which allow strong light–matter interactions, enabling the precise control of the electromagnetic response of the metamaterial. Typical geometries include split-rings resonators, fishnets or metallo-dielectric multilayers. Among these, a sub-class of metamaterials called plasmonic nanorod metamaterials, has received a lot of interest because of its unique optical properties, related to the realization of hyperbolic optical dispersion and an epsilon-near-zero regime.

Hyperbolic optical metamaterials are uniaxial anisotropic metamaterials with dielectric permittivities along the major optical axes having different signs. As opposed to conventional materials showing closed elliptic isofrequency surfaces, hyperbolic metamaterials, in a theoretical limit of negligible losses and infinitely small unit cells, exhibit open hyperbolic isofrequency surfaces for extraordinary waves, thus supporting propagating waves with high wavevectors in the directions close to the hyperbolic asymptotes, which otherwise would typically be evanescent in conventional media. Practical realizations of hyperbolic metamaterials include planar systems, such as metal-dielectric multilayers[8,13–16] and plasmonic nanorod arrays.[17,18] The extension of these platforms to nanoparticle architectures by structuring multilayer or nanorod metamaterials, or the creation of multishell nanoparticles has been also proposed.[16,19–21]

Due to their unique optical properties, tuneable from the UV spectral range to the NIR by choosing appropriate materials and geometrical parameters,[22] hyperbolic metamaterials have so far been used in a variety of applications, including subwavelength imaging,[5] sensing[23] and spontaneous emission engineering[24] as well as ultrafast all-optical switching[25] and polarization control.[26] Hyperbolic metamaterials operating in the radio-frequency spectral range have also been demonstrated.[27] Recently, naturally occurring hyperbolic materials[28,29] have attracted great interest, especially low-dimensional (2D) materials.[30–32] Taking advantage of the hyperbolic dispersion, these materials support hyperbolic plasmon-polaritons (HPP),[33–35] as, e.g., black phosphorus and tungsten ditelluride, and hyperbolic phonon-polaritons (HPhP),[36–38] as,
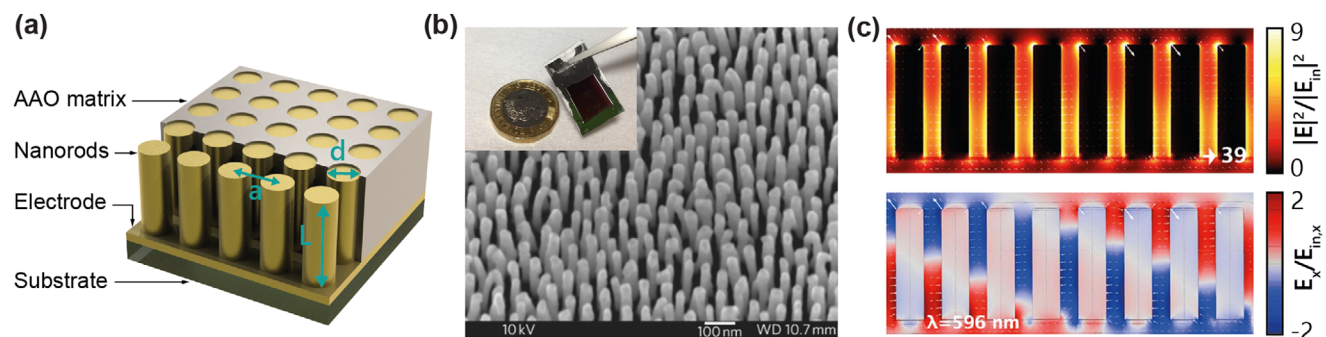
Figure 1. a) Schematics of a nanorod metamaterial in an AAO matrix. b) SEM image of a plasmonic nanorod-based metamaterial tilted at 45°. Inset: Photograph of a typical sample and a pound coin for scale. Reproduced with permission.[25] Copyright 2011, Macmillan Publishers Limited. c) Near-field intensity map (top panel) and the distribution of the E_x component (normal to the nanorod axis) of the electric field (bottom panel) inside the nanorod metamaterial in the hyperbolic dispersion regime, under excitation with TM-polarized light at oblique incidence, illustrating electromagnetic coupling between the nanorods. Reproduced with permission.[62] Copyright 2019 IOP Publishing Ltd.

e.g., hexagonal boron nitride and α-phase molybdenum trioxide, to name but a few.

Plasmonic nanorod metamaterials can exhibit both hyperbolic and elliptical dispersion depending on the operational wavelength and light polarization. Particularly, for TM-polarized light the change from one type of dispersion to the other happens at a certain wavelength called the epsilon-near-zero (ENZ) point, at which the sign of the metamaterial effective dielectric permittivity along the nanorods changes from positive to negative. In recent years, the behavior of materials (e.g., conducting oxides) and metamaterials (e.g., with nanorod and multilayer designs) in the ENZ regime has attracted increasing interest thanks to their enhanced performance in all-optical[25,39,40] and electro-optical modulation,[41–43] all-optical control of harmonic generation,[44] sensing,[45] and light emission.[46]

In this review, we report on the optical properties and applications of plasmonic metamaterials based on aligned metallic nanorod assemblies. After a brief description of their fabrication process, based on a scalable self-assembly technique, the microscopic and effective medium descriptions of the nanorod-based metamaterials will be discussed, including both local and nonlocal theories. The role of the nonlocal response of the metamaterial on its dispersion will be highlighted. We will then focus on the multi-scale structuring of the nanorod-based metamaterials into finite-size components such as photonic-crystal-like structures, resonators or waveguides, allowing for further control of their optical response and additional functionalities. The nonlinear properties of the plasmonic nanorod metamaterial will then be discussed, together with how these nonlinearities can be exploited in novel applications. The great variety of applications of nanorod-based metamaterials, ranging from sensing to spontaneous emission engineering, will then be described, and the development of novel anisotropic plasmonic metamaterial designs, derived from the nanorod-based architectures, will be presented. Finally, the fast-developing trends in the exploitation of these metamaterials in novel nanophotonic concepts will be outlined.

2. Fabrication Approaches

The nanorod-based metamaterials are typically fabricated by electrochemical growth of metals (or semiconductors) into a porous

anodized aluminum oxide template (AAO).[17,47,48] As depicted in **Figure 1a**, the nanorod metamaterials are usually manufactured on a supporting glass (with a thin tantalum pentoxide layer for adhesion) or silicon substrate, with a thin gold film acting as an electrode for the electrochemical deposition in either case. An aluminum film with a thickness of several hundreds of nanometers is then formed by magnetron sputtering and subsequently anodized to produce the porous AAO template. The pore diameter (denoted d), separation (denoted a) and ordering can be controlled by the anodization conditions, including the voltage applied and the type of acid used as the electrolyte, as well as the post-chemical etching processes. This anodization process results in a highly-ordered quasi-periodic hexagonal array of pores. Nanopore diameters ranging from 20 to 80 nm and inter-pore distances in the range of 40–100 nm can typically be obtained. A perfect hexagonal lattice can be achieved with a two-step anodization process or by prestructuring the aluminum film with a "seed" indentation pattern using focused-ion-beam or electron-beam lithography,[49] which, however, is more time-consuming and increases the cost of the final structure. The plasmonic nanorod system is then finally fabricated by electrodeposition of the nanorod material into the nanopores, with the time of the electrodeposition determining the length of the nanorods (denoted L). Any material suitable for electrodeposition including but not limited to Au,[17] Ag,[50] Cu,[51] Ni,[17,52] or TiN[51] can be used. Recent research has also shown the possibility of electrodepositing semiconductors, e.g., zinc oxide.[53] The AAO template can also be completely etched away in order to obtain free-standing nanorods.

Figure 1b shows a SEM image of a nanorod metamaterial and a photograph of a typical cm²-size sample. This self-assembly technique allows to fabricate uniformly nanostructured metamaterial layers over very large macroscopic areas. At least for some materials (e.g., Cu in an ITO matrix), the nanorod metamaterial can also be prepared by solid-state mixing, followed by a sintering process, which makes the fabrication cheaper but at the cost of a decreased quality of the structure.[54] Inclined Al and TiN nanorod metamaterials were obtained by an oblique deposition technique.[55,56] Alternatively, traditional self-assembly methods based on chemical functionalization can be used,[57–59] which are low-cost, but accompanied by somewhat lower quality.

Oppositely, electron beam lithography can be employed to fabricate high-quality/high-cost nanorod metamaterials with the restriction on critical sizes and overall metamaterial area.[60] Self-assembly-mask etching was used to fabricate silicon hyperbolic nanorod metamaterials.[61]

Structuring of the metamaterial to create multiscale structures combining sub-wavelength size nanorods and wavelength-scale features can be achieved at various steps of the self-assembly/electrodeposition fabrication process: before anodization, using an imprinting procedure to define the spots of the nanopore growth; after the anodization but before the electrodeposition, by controlling the AAO pores opening by a focused ion beam; or after electrodeposition and removal of the AAO matrix, by laser ablation.[63] The inexpensive and relatively easy fabrication process of plasmonic nanorod metamaterials, using the above self-assembled approach combined with the ability to tune their geometrical parameters, allows their electromagnetic properties to be tailored in a wide spectral range and over large areas.

3. Effective Medium Theory and Microscopic Description of the Optical Properties

3.1. Local Effective Medium Theory

As the spacing between the meta-atoms is commonly subwavelength or/and randomized, the diffraction effects are absent and light propagates through the metamaterial as through a uniform medium with effective optical properties (Figure 1c). The essence of the metamaterial approach is that these optical properties are designed through engineering the optical response of the individual meta-atoms and electromagnetic coupling between them. The effective permittivity and permeability of the metamaterial are derived using effective medium theories (EMTs) based on homogenization of the metamaterial optical behavior. In the case of nanorod metamaterials, the homogenization can be done by straightforward averaging of the displacement $\langle \mathbf{D} \rangle$ and the electric $\langle \mathbf{E} \rangle$ fields over the metamaterial volume, followed by taking a ratio of the outcomes along the major metamaterial axes, as $\langle \mathbf{D} \rangle = \varepsilon_{\text{eff}} \langle \mathbf{E} \rangle$.[64] Generally, the nanorod metamaterial behaves as a highly anisotropic uniaxial medium with the optical axis directed along the nanorods and the effective dielectric permittivity given by a diagonal tensor[8,64–66]

$$\epsilon_{\text{eff}} = \begin{pmatrix} \epsilon_{\text{eff},\perp} & 0 & 0 \\ 0 & \epsilon_{\text{eff},\perp} & 0 \\ 0 & 0 & \epsilon_{\text{eff},\parallel} \end{pmatrix} \tag{1}$$

where

$$\epsilon_{\text{eff},\perp} = \epsilon_{\text{d}} \frac{(1+f)\epsilon_{\text{m}} + (1-f)\epsilon_{\text{d}}}{(1-f)\epsilon_{\text{m}} + (1+f)\epsilon_{\text{d}}} \tag{2}$$

and

$$\epsilon_{\text{eff},\parallel} = f\epsilon_{\text{m}} + (1-f)\epsilon_{\text{d}} \tag{3}$$

are the permittivity components perpendicular and parallel to the optical axis, respectively, calculated using the EMT and defined by the dielectric permittivities of the metal (ϵ_{m}) and the surrounding

dielectric (ϵ_{d}), together with the metal filling factor f. In the case of a hexagonal nanorod arrangement $f = \pi d^2/(4a^2\sin(\pi/3))$.

The spectral dependencies of the real and imaginary parts of the dielectric permittivity components are plotted in **Figure 2a**. The characteristic double-bending in the real part of $\epsilon_{\text{eff},\perp}$ together with the corresponding peak in its imaginary part are related to the transverse plasmonic resonance of the nanorods slightly spectrally shifted due to their electromagnetic coupling. The real part of $\epsilon_{\text{eff},\perp}$ can be either positive throughout the spectrum, or, in the case of small losses, can reach negative values near its minimum. The real part of $\epsilon_{\text{eff},\parallel}$ on the other hand represents a weighted sum of the permittivities of the metal and the surrounding dielectric with coefficients defined by the metal filling factor f. It logically follows that at short wavelengths it is positive, while at long ones it becomes negative due to large negative values of ϵ_{m} in this spectral range. The spectral interval around the point where $\epsilon_{\text{eff},\parallel}$ crosses zero is called the epsilon-near-zero (ENZ) region. The effective permeability of the nanorod metamaterial is equal to 1 because, by design, the metamaterial does not produce any artificial magnetic response and its constituting materials (like all other materials considered here) are non-magnetic at optical frequencies.

For the ordinary wave (excited by TE-polarization of the light and experiencing only the $\epsilon_{\text{eff},\perp}$ component), the metamaterial behaves as a lossy dielectric (or a metal if $\epsilon_{\text{eff},\perp}$ becomes negative) with a spherical dispersion. Here, TE-(TM-) polarization corresponds to the arrangement where the electric (magnetic) field of the incident wave is perpendicular to the plane of incidence. In the case of the extraordinary wave, excited by TM-polarized light, the metamaterial behaves as a lossy dielectric with an elliptic dispersion at shorter wavelengths than the ENZ point, located at around 700 nm for the metamaterial parameters illustrated in Figure 2a. Above the ENZ point, the dispersion of the extraordinary wave becomes hyperbolic, giving the name for this type of metamaterials. In the elliptic regime, the optical anisotropy Δn, i.e., the difference between ordinary and extraordinary refractive indices, in the visible and NIR spectral ranges, is comparable to the best natural anisotropic materials ($\Delta n \sim 0.2$), while in the hyperbolic regime, ($\Delta n \sim 1.5$) far exceeds what is possible to achieve in conventional materials.[68] With another choice of geometrical and material parameters, the hyperbolicity can also occur when $\epsilon_{\text{eff},\perp}$ reaches negative values.[69] Natural hyperbolic materials also exist,[28,29] but they are fundamentally non-tuneable and very rare in the vis/NIR spectral range.

In the limit of zero losses and an infinitely small unit cell, the isofrequency dispersion of nanorod plasmonic metamaterial is presented by a hyperbola infinitely extending in the k-space (Figure 2a). For realistic losses, the dispersion surface evolves into a hyperbola-like closed shape for which the wavevectors above a certain value are cut off.[70] Another factor limiting the magnitude of the allowed wavevectors is a breakdown of the EMT at $k \sim 1/a$, when diffraction effects become important for finite-size unit cells.

One may note that there is another homogenization approach based on the derivation of the effective optical properties of a metamaterial layer of a finite height from both transverse and longitudinal resonances of the nanorods (having in this case a finite length).[71] Therefore, the homogenization should be repeated every time the nanorod length (thickness of the metama-
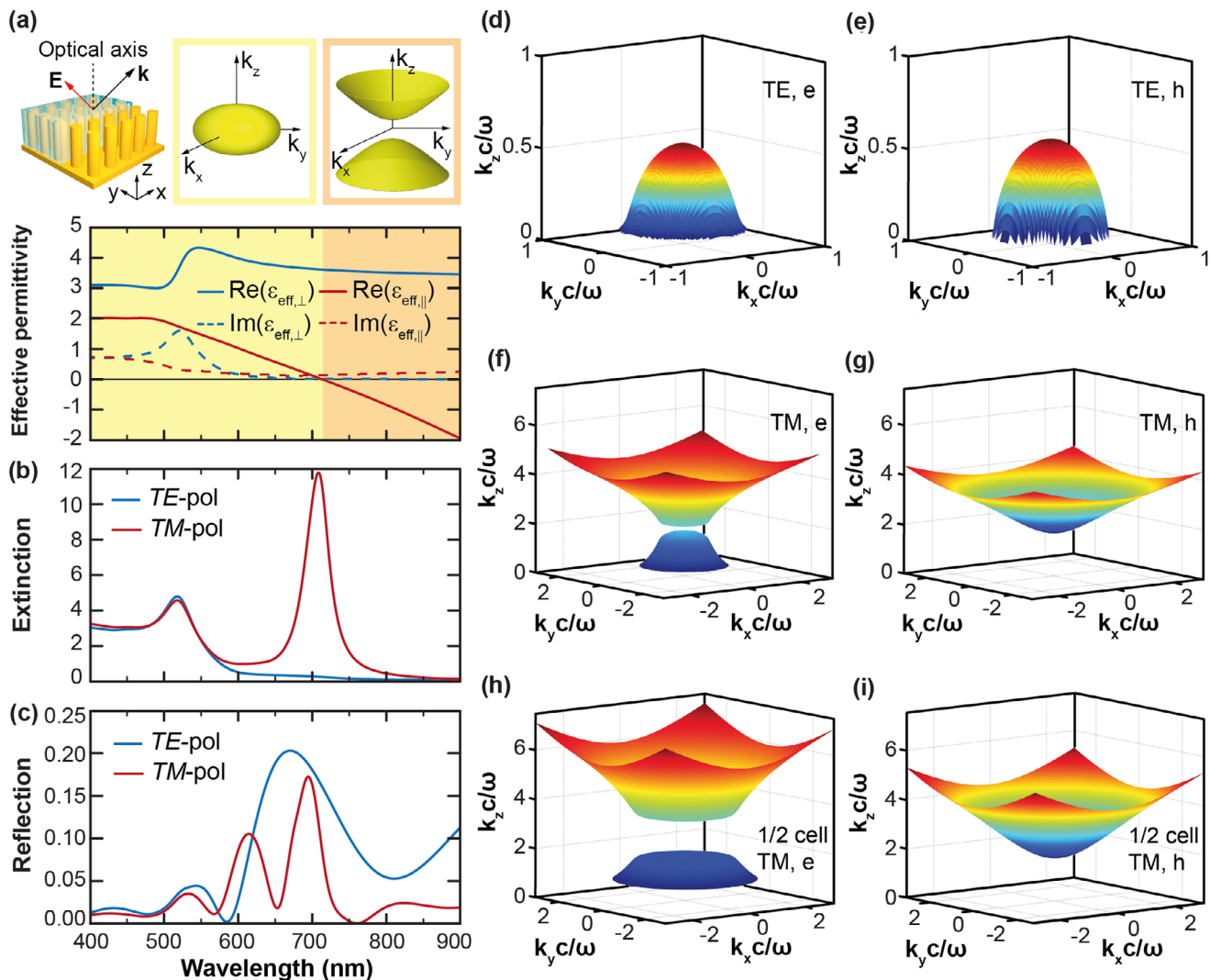
**ADVANCED
SCIENCE NEWS**

www.advancedsciencenews.com

www.lpr-journal.org

LASER
& PHOTONICS
REVIEWS

Figure 2. a) Spectral dependences of the real and imaginary parts of the components of the effective permittivity tensor of the metamaterial produced by a hexagonal array of gold nanorods ($d = 30$ nm, $a = 80$ nm) in a dielectric matrix ($n = 1.6$). The regions of elliptic (yellow) and hyperbolic (orange) dispersion of the extraordinary wave (excited by TM-polarized illumination) are indicated, together with the corresponding isofrequency dispersion plots in the color-matched boxes. b,c) Extinction ($-\ln(T)$, where T is the transmission) (b) and reflectivity (c) of a metamaterial layer with a thickness of 450 nm, described by the effective permittivity presented in (a), illuminated with TE- and TM-polarized waves at the incidence angle of 30°. Reproduced with permission.[8] Copyright 2022, American Chemical Society. d–i) Isofrequency surfaces of TE (d,e) and TM (f–i) modes supported by the nanorod metamaterial calculated using the nonlocal effective medium theory in (d,f,h) elliptic (denoted e) and (e,g,i) hyperbolic (denoted h) regimes for (d–g) a metamaterial with $d = 50$ nm, $a = 100$ nm and (h,i) metamaterial with 50% decreased parameters ($d = 25$ nm, $a = 50$ nm). Such scaling does not change the metamaterial optical properties calculated using the local effective medium but has a strong impact in the nonlocal case. Reproduced with permission.[67] Copyright 2017, Springer Nature.

terial layer) is changed. Although this approach predicts the existence of the ENZ point discussed above, it also stipulates the presence of a second one, after which $\epsilon_{eff,\parallel}$ returns to positive values at longer wavelengths. This is most probably due to essentially treating the assembly as a 3D system of oriented, but uniformly dispersed nanorods and, therefore, disregarding their side-to-side arrangement in the derivation of this EMT. Overall, both hyperbolicity and ENZ effects, being very exotic characteristics, play a very important role in the observed optical phenomena and related applications of nanorod-based metamaterials. Importantly, these effects can be tuned throughout the visible and infrared

spectral ranges by controlling the geometrical parameters of the nanorods at the fabrication stage,[72] with possible extension to the ultraviolet region with the use of high plasma frequency metals, such as aluminum.

For transmission, reflection and absorption, the optical response of the metamaterial layer directly follows from its effective permittivity and can be calculated, e.g., using the transfer matrix method as for any other planar film geometry (Figure 2a). As was explained above, ordinary waves excited by TE-polarization of the incident light propagates through the metamaterial as through a lossy dielectric with a spherical dispersion, while the extraor-

dinary waves excited by TM-polarized light experience elliptic or hyperbolic dispersion, depending on their frequency. For an incident light with either TE- or TM-polarization states (i.e., the ordinary and extraordinary waves), either of which have an electric field component across the nanorod, the extinction spectrum (Figure 2b) shows a peak at the wavelength of 520 nm (for the chosen typical geometrical/material parameters). This peak corresponds to the excitation of the coupled transverse resonances of the nanorods and matches the peak position in Im($\epsilon_{\text{eff},\perp}$). For the extraordinary wave excited by TM-polarized illumination, there is an electric field component along the nanorods (along the optical axis of the metamaterial), experiencing $\epsilon_{\text{eff},\parallel}$. As a consequence, another extinction peak appears at the spectral position of the ENZ point,[73] related to the fact that at the ENZ condition, the propagation of a TM-polarised wave inside the metamaterial is significantly hindered by high attenuation, independently of the angle of incidence.[66] The increase in the incidence angle, resulting in an increase of electric field component parallel to the nanorods, leads to a monotonic rise of the magnitude of the ENZ extinction peak. Away from the regions of high extinction, Fabry–Pérot effects or waveguided modes can be observed in reflection (Figure 2c) or transmission of a metamaterial slab (see Section 4 for further details).

3.2. Nonlocal Effective Medium Theory

The independence of the spectral position of the ENZ-related extinction peak on the angle of incidence of the TM-polarized wave and its monotonic increase with the increase of this angle, predicted by the EMT discussed above, raises a question about the limits of its validity, as it was experimentally shown that for nanorods made of a plasmonic material with low losses, the behavior of the ENZ peak experiences an angle-dependent spectral splitting.[66] This peculiar disagreement between the EMT and the experiment was resolved by considering the microscopic nature of the interaction of light with the metamaterial taking into account nonlocal (spatial dispersion) effects induced by the nanostructuring.[74] These effects are not captured by the local EMT described above, but automatically taken into account in full vectorial numercal modelling. The nonlocal effects in the EMT description are related to interacting cylindrical plasmons supported by the nanorods and propagating along them. Due to the symmetry of the modes, all the components of the electric and magnetic fields are averaged out over the metamaterial unit cell, apart from the E_z one. Thus, macroscopically, the resulting mode (a sum of 0-, 4-, 8-,.. order cylindrical plasmons in individual nanorods) presents a longitudinal plane wave propagating along the z-direction. Within the EMT approach, this wave can be readily taken into account introducing nonlocality into the $\epsilon_{\text{eff},\parallel}$ component of the effective permittivity tensor. Particularly, the nonlocality is introduced by the dependence of the permittivity on the wavevector k_z. The nonlocal expression for $\epsilon_{\text{eff},\parallel}$ is obtained by matching the dispersion of the longitudinal wave in the nonlocal EMT medium to the dispersion obtained from the microscopic description of the collective cylindrical plasmon mode, via setting the proper asymptotic behavior at long-wavelengths and also reproducing the local EMT expression in the limiting case of small wavevectors. For the derived nonlocal permittivity

tensor, the TE-polarized ordinary waves keep their behavior, unaffected by the changes in $\epsilon_{\text{eff},\parallel}$, but the TM-polarized extraordinary waves, which have an electric field component along the nanorods, upon coupling with the nonlocal longitudinal mode, produce two hybridized TM-polarized waves. The dispersions of these modes produce a typical anticrossing pattern, happening in the ENZ region. The splitting of the modes becomes more pronounced with the decrease of the losses in the nanorods, which explains how the extinction of the metamaterial at the ENZ is altered in the case of constituent materials with different losses.

The impact of the nonlocality on the isofrequency dispersion surfaces is presented in Figure 2d–i. As expected, the TE-polarized modes are unaffected by the nonlocality and keep their elliptic dispersion. For the TM-polarized case, in the hyperbolic wavelength range (Figure 2g), the dispersion also keeps its generic hyperbolic topology, while in the ENZ and elliptic wavelength range (Figure 2f) the formation of the two TM modes is clearly visible. The nonlocality significantly affects other optical phenomena, including spontaneous emission inside the metamaterial, which will be discussed in detail below. The approach described above can be reformulated through the k-dependence of the effective susceptibility of the metamaterial.[66,75] An alternative nonlocal EMT, although taking into account essentially the same physical phenomenon, is derived in ref. [76]. Finally, one needs to stress that the nonlocality related to spatial dispersion in all the EMT theories considered here, is produced by the nanostructuring of the metamaterial, but not by the nonlocality of the optical properties of the materials constituting it. The role of nonlocality and the need for microscopic description is especially important for consideration of effects associated with the internal fields inside the metamaterial, such as related to spontaneous emission from molecules located inside it or nonlinear effects in the nanorods, since the local EMT fails to take into account strong variation of the fields within the unit cell arising due to the excitation of cylindrical surface plasmons. The influence of nonlocal effects on Cherenkov radiation inside a hyperbolic layered metamaterial has been studied in ref. [77]. While numerical simulations reproduce the optical properties of nonlocal metamaterials, the consideration of the nonlocal EMT allows to understand physical processes inside the metamaterial and its optical mode structure.

As was mentioned above, the nonlocal effects are particularly pronounced in the ENZ region. In this regime, the TM-polarized light incident on the metamaterial efficiently couples to both TM modes supported by the nonlocal metamaterial, despite these modes having significantly different dispersion characteristics. Thus, light transmitted through the metamaterial effectively perceives it as a highly spectrally and spatially dispersive medium. Furthermore, as the coupling coefficients to the TM modes are highly angular-dependent, the resulting effective dispersion can be controlled by simply changing the angle of incidence. Particularly, using this approach it has been experimentally shown that light propagation can be switched between backward, slow-light and superluminal regimes.[78] It has been also shown that due to the ENZ-related strong effective dispersion, the metamaterial can be used as a dispersion management device with a THz bandwidth, capable of producing both positive and negative chirps of light pulses.
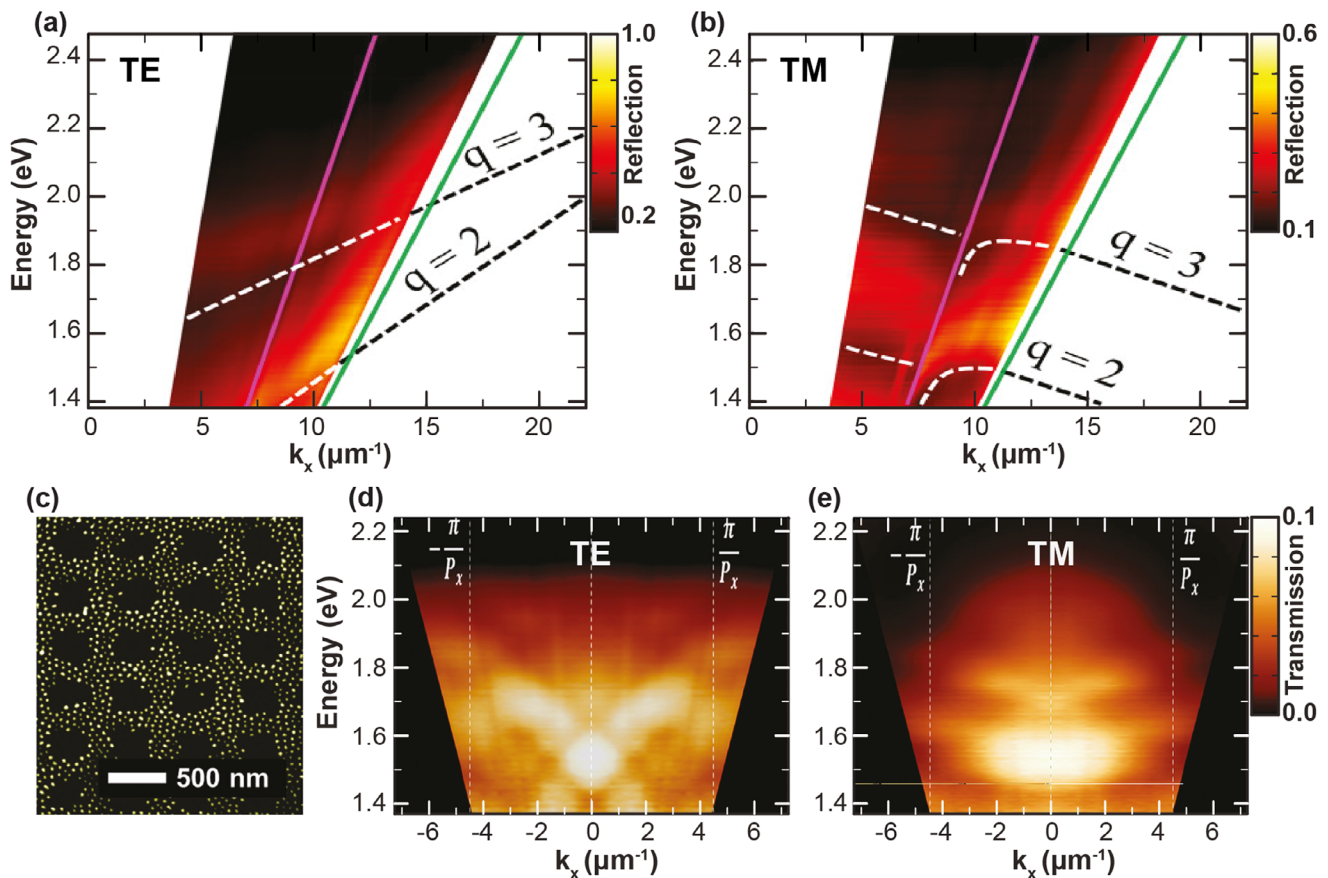
Figure 3. a,b) Experimentally measured reflectance from a 340 nm thick metamaterial slab, showing the dispersion of guided plasmonic modes (nanorod filling factor 0.32, period ≈100 nm, and radius ≈32 nm) for (a) TE and (b) TM modes. The second and third order guided modes are marked with dashed lines and the light lines in the silica substrate and the air superstrate are plotted in green and magenta, respectively. Reproduced with permission.[82] Copyright 2015, Wiley-VCH. c) SEM image of a periodically structured nanorod metamaterial. d,e) Experimentally measured transmission through the nanostructured metamaterial slab with a design presented in (c), showing the dispersion of the Bloch modes (nanostructuring period 700 nm, patch size 300 nm) for: (d) TE and (e) TM modes. Reproduced with permission.[85] Copyright 2015, Wiley-VCH.

4. Metamaterial Waveguides and Polaritonic Crystals

Metamaterials and metasurfaces have been attracting considerable attention for the manipulation of light in 2D and 1D waveguided geometries.[79–81] Similarly, a nanorod metamaterial slab may work as a resonator or a waveguide for optical modes propagating inside it. For plasmonic nanorod metamaterials, these modes are sometimes called bulk plasmonic modes or volume plasmonic modes since, in the microscopic description, they are related to the electron plasma oscillations in the nanorods. The presence of these modes defines the metamaterial slab reflection and transmission through the formation of Fabry–Pérot-type interference patterns (Figure 2c).[82,83] In extinction, though, their presence is hidden by the two dominating peaks of the transverse plasmonic resonance (short-wavelength peak) and the ENZ attenuation (long-wavelength peak). When the metamaterial slab is illuminated in the attenuated total internal reflection geometry, leaky waveguided modes can be excited.[82,83] True waveguided modes are also supported by the metamaterial, but to match the very long wavevector of these modes, their excitation from the far-

field requires special arrangements, e.g., a diffraction grating, or an emitter inside the metamaterial slab.

In a planar nanorod metamaterial slab waveguide, TE modes (having their electric field in the waveguide plane and perpendicular to the propagation direction), for which the components of the nanorod metamaterial permittivity tensor are commonly positive, can be viewed as typical modes in a lossy dielectric waveguide. This also applies to the TM modes (having their magnetic field in the waveguide plane and perpendicular to the propagation direction) in the short-wavelength spectral range, where the z-component of the metamaterial effective permittivity is positive (Figure 2a). At the longer wavelengths, above the point where the z-component of the effective permittivity becomes negative (which can be viewed as a spectral point defining an effective plasma frequency of the nanorod metamaterial for this component), the TM modes take the form of bulk plasmon–polaritons propagating in a hyperbolic anisotropic medium[82] (**Figure 3a,b**). The TM modes show particularly interesting properties. These modes may have a very low or negative group velocity with high effective refractive indices (up to 10), while their unusual high-frequency cut-off provides

**ADVANCED
SCIENCE NEWS**

www.advancedsciencenews.com

**LASER
& PHOTONICS
REVIEWS**

www.lpr-journal.org

deep-subwavelength ($\lambda_0/6 - \lambda_0/8$ waveguide thickness) single-mode guiding.[82] It is worth underlining that the guiding properties of the nanorod slab metamaterial waveguides, and particularly the dispersion of the modes, can be engineered at the fabrication stage. Hyperbolic metamaterials can be further exploited to achieve 3D waveguides with unusual properties. While in the case of the slab waveguide the TE and TM modes are independent, 2D confinement makes them coupled, which leads to the formation of hybrid guided modes at the TE–TM crossing points of the dispersion.[84] Such modes show very strong group velocity dispersion with slow or stopped light behavior.

To achieve further control over the dispersion of the modes supported by the metamaterial, one can adopt an approach inspired by photonic crystal geometries, in order to implement hyperbolic polaritonic crystals (HPCs) by introducing periodic structuring of the nanorod metamaterial at a wavelength scale (Figure 3c).[85] In this way, the multiscale arrangement of the nanorods is achieved with two distinct geometrical sizes: the sub-wavelength distance between the nanorods and the periodicity of nanorod patches. This gives the opportunity to engineer the guided properties both intrinsically via the design of the metamaterial and extrinsically via the profile of the nanostructuring. The TE HPC modes show the usual Bloch behavior conditioned by the periodic nanostructuring with back-bending and splitting at the edges of the Brillouin zones, while for the TM modes this effect is less pronounced due to their almost dispersionless behavior (Figure 3d,e). Apart from allowing additional flexibility for the control of the plasmonic modes behavior, the additional momentum provided by the nanostructuring enables optical access to these modes. Such modes are normally unreachable via conventional or attenuated total reflection methods due to their high effective indices, while they are very important, e.g., for the engineering of spontaneous emission.

5. Sensing Applications

Due to their high sensitivity to variations in the refractive index of the surrounding environment, plasmonic nanorod metamaterials have been shown to be extremely useful in various types of sensing applications, outperforming typical surface plasmon polariton and localized surface plasmon based sensors.[8,86,87] Used for biosensing and chemical compound identification as well as active nanophotonic devices, the extreme sensitivity of this type of systems is provided by a modification of the optical properties of the metamaterial originating from the changes in the optical response of individual nanorods and interaction between them, which results in an alteration of the mode structure supported by the metamaterial.

5.1. Biosensing

Improvement in biosensing technology has been demonstrated using a gold nanorod-based metamaterial supporting leaky waveguided modes.[23] The guided mode of interest, excited by TM-polarized illumination in the hyperbolic dispersion regime, is represented by an angular-dependent dip in attenuated-total-reflection intensity around the wavelength of 1200 nm

(**Figure 4a**). The field of the mode is primarily located within the metamaterial slab, where strong confinement of the electromagnetic field is observed. Therefore, the mode is particularly sensitive to the changes of the refractive index of an analyte filling the space between the nanorods. The specific functionalization of the nanorod surfaces with, for instance, antibodies of the biospecies targeted for the detection links them to the nanorods, where upon the consequent change of the refractive index in the inter-rod area, they can be detected by a spectral shift of the guided mode in the attenuated reflection spectrum of the metamaterial. Particularly, this metamaterial platform provides enhanced sensitivity to refractive index changes, leading to unprecedented sensitivities of 10000s nm per refractive index unit.[23,88] The nanorod metamaterial sensing platform can be further enhanced by creating sub-attoliter shells around the nanorods by etching the AAO matrix for the introduction of analytes.[89] Importantly, the nanorods provide large surface area for functionalization. Nanorod-based metamaterials have also recently been used as a platform to improve sensing and identification of chiral molecules, via the enhancement of the circular dichroism response of molecules placed in between the nanorods.[90]

5.2. Gas Sensing

The plasmonic nanorod metamaterial has widely been used in the context of gas sensing, offering an all-optical platform for hydrogen detection.[91] The design based on a hybrid gold-core/palladium-shell structure has shown more than a 30% change in both reflection and transmission of the metamaterial layer in a 2% hydrogen in a nitrogen environment, observable even by the naked eye (Figure 4b). The high sensitivity to the presence of hydrogen stems from the formation of palladium hydride, inducing both a change of the material properties of the individual nanorods and a modification of the shell thickness, which leads to a change of the effective permittivity of the metamaterial and, therefore, of the modes supported by the structure. Reusability of the sensor is ensured by the fast reset of the system, thanks to the reversible phase transition from palladium to palladium hydride. This all-optical sensing device also constitutes a safer option compared to its electric counterparts, eliminating the presence of electric circuitry in hydrogen environments and therefore minimizing the risk of explosion.

Sensing of oxygen and hydrogen gases has also been demonstrated using the highly reactive tunnel junctions based on electrically driven plasmonic nanorod metamaterials[92] (Figure 4c). The metamaterial provides an opportunity to achieve a very high density ($\sim 10^{11} \text{cm}^{-2}$) of tunnel junctions with a top tip of each nanorod acting as one of the contacts. In addition to the dominating process of elastic tunneling when electrons tunnel through the gap without energy loss, upon inelastic tunneling electrons excite the optical modes supported by the metamaterial and metal-insulator-metal modes in the tuneling gaps of individual nanorods, with the efficiency determined by the partial local density of optical states corresponding to each of these modes.[94,95] Due to the extreme sensitivity of the tunneling process to any changes in the nanometer-scale tunneling gap, the introduction of gas molecules in the active area inside the gap affects the
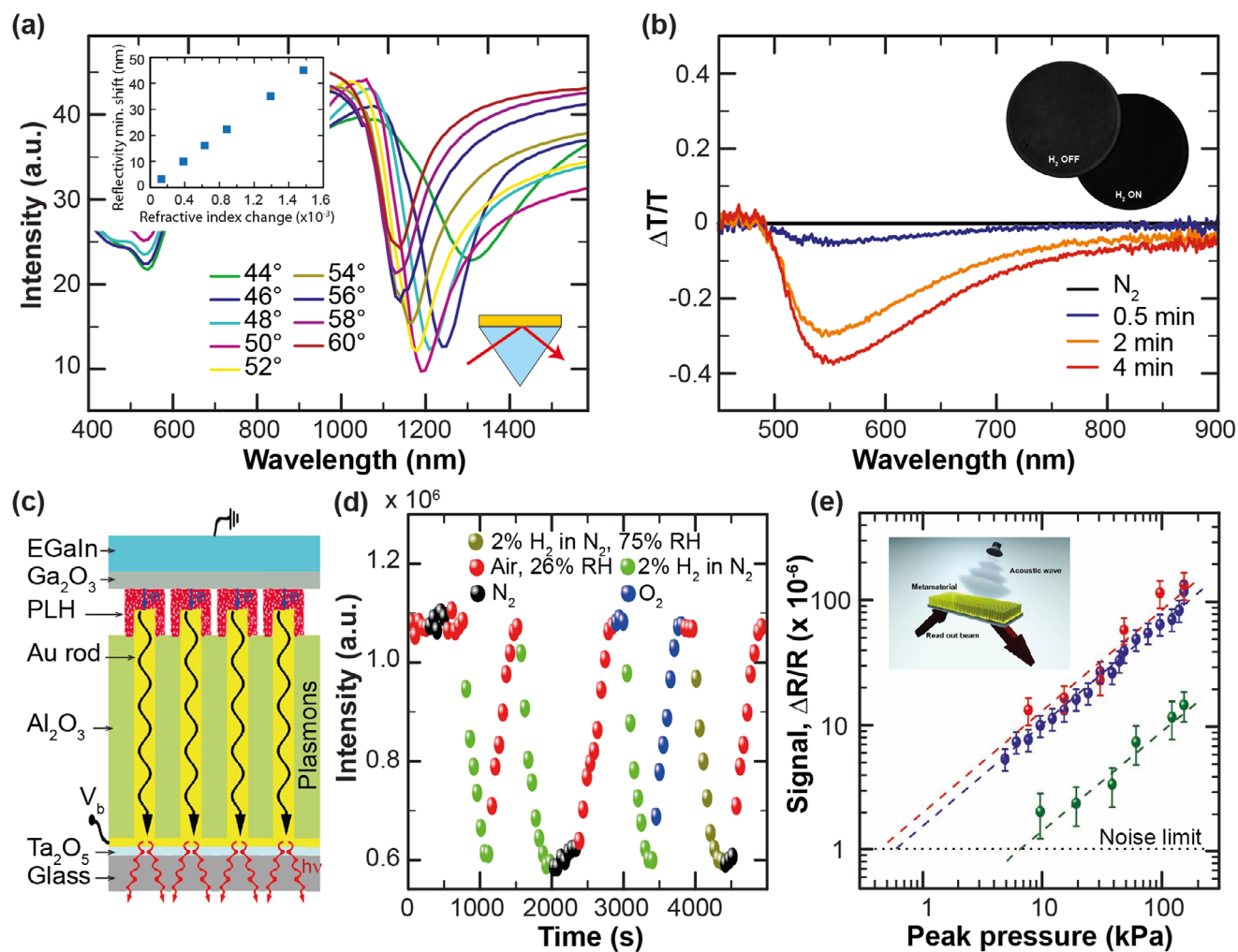
ADVANCED
SCIENCE NEWS

www.advancedsciencenews.com

LASER
& PHOTONICS
REVIEWS

www.lpr-journal.org

Figure 4. a) Reflection spectra of a nanorod metamaterial in an aqueous environment ($n = 1.33$), obtained in an attenuated total reflection geometry for various angles of incidence. The nanorod metamaterial parameters are 380 nm length, 25 nm diameter, and 60 nm center-to-center spacing. Reproduced with permission.[23] Copyright 2009, Macmillan Publishers Limited. b) Variation of transmission (TM-polarized illumination, angle of incidence ≈40°) of the metamaterial on the exposure to 2% hydrogen gas in nitrogen. Inset: Transmitted intensity in the absence and the presence of hydrogen: the brightness is significantly reduced on the hydrogen exposure. Reproduced with permission.[91] Copyright 2014, Wiley-VCH. c) Schematic diagram of a device configuration based on metal-polymer-metal tunnel junctions. The Al_2O_3 matrix was first chemically etched to expose the Au nanorod tips. The nanorod tips were then functionalized with a monolayer of poly-L-histidine (PLH) that works both as a tunnel barrier and a reactant. Finally, an EGaIn electrode was formed on the top of the structure. d) Integrated emission power from the metamaterial measured when the cell atmosphere was dynamically changed between air, N_2, 2% H_2 in N_2, O_2, and 2% H_2 in N_2 with 75% relative humidity. Reproduced with permission.[92] Copyright 2018, Macmillan Publishers Limited. e) Dependence of the reflectivity on the acoustic pressure for metamaterial sensors (red and blue) and a reference SPR-based sensor (green). The operational wavelength is 600 nm; the probe light is TM-polarized and incident at 45°. The SPR sensor is based on a 50 nm Au film. The noise limit of the detection system which determines the sensitivity is also indicated. Reproduced with permission.[93] Copyright 2013, Wiley-VCH.

excitation of the above modes and, therefore, light radiated after their outcoupling , as well as the tunneling current. Particularly, oxygen or hydrogen produces the corresponding oxidation or reduction reactions in the gold and polymer, assisted by hot electrons produced via elastic tunneling, which were detected both electrically and optically by observing the light produced by out-coupling of the excited modes at the opposite metamaterial interface as well as the changes in the tunneling current (Figure 4d). Even in a non-optimized case, the sensitivity for hydrogen molecule detection was about two times higher than the one obtained with the gold-core/palladium shell structures, highlighting the potential of such platforms for highly sensitive sensing applications.

The sensitivity of the plasmonic nanorod metamaterial to the changes in the environmental humidity can be explained by the roughness-assisted formation of a nanoscale water layer on the surface of the nanorods. On the one hand, this can be used for optical sensing of relative humidity and on the other, it indicates the importance of considering the humidity conditions for optical characterization of plasmonic nanostructures and most importantly for the design of sensors based on them.[96]

**ADVANCED
SCIENCE NEWS**

www.advancedsciencenews.com

LASER
& PHOTONICS
REVIEWS

www.lpr-journal.org

5.3. Ultrasound Detection

Any kind of refractive index variations of the media between the nanorods, not only related to the presence of an analyte substance within the metamaterial slab, can be efficiently detected. This was exploited for ultrasensitive detection of ultrasound.[93] In this case, gold nanorods in a polymer matrix were subjected to the pressure of an ultrasound pulse generated via a photo-acoustic effect. Acoustic waves could be sensed from the pressure-induced variations of the refractive index of the polymer, leading to a frequency shift of the ENZ point of the metamaterial. Together with large bandwidth and a sub-nanosecond response time, sensitivity levels of less than 500 Pa were achieved, corresponding to a detection limit at least an order of magnitude better than piezoelectric or surface plasmon resonance-based sensors (Figure 4e).[97,98] The non-resonant and, therefore, significantly broadband character of this sensing mechanism offers more flexibility in terms of design and optimization of the sensors compared to their resonant counterparts. This makes metamaterial-based acoustic sensors a promising alternative to conventional sensors for photo-acoustic imaging systems and related biomedical applications.

6. Nonlinear Optical Properties

Nonlinear optical phenomena are proportional to the higher powers of the driving field, e.g., the second power for the second harmonic generation (SHG) as it is a second-order process. Thus, plasmonic nanostructures and metamaterials present a unique platform for the enhancement of nonlinear processes, as they offer a very large increase in the magnitude of local electromagnetic fields. One of the approaches to enhance a generally weak nonlinear response of conventional nonlinear materials is to hybridize them with plasmonic nanostructures to exploit the field enhancement effect.[99,100] An alternative approach utilizes the fact that metals are themselves intrinsically nonlinear materials offering one of the largest nonlinearities, in this case provided by the free-electron gas.[101] These nonlinearities can be further enhanced by a particular design of plasmonic nanostructures or metamaterials.[102–105]

6.1. Second-Harmonic Generation

The second-order nonlinear response of centrosymmetric materials, including metals, is forbidden due to symmetry considerations, with only weak surface SHG allowed as the symmetry breaks at the interface. However, surface SHG can be boosted by the local field enhancement provided by plasmonic nanostructures. Nanorod-based metamaterials, in this respect, represent an interesting system thanks to the large metal surface area of the nanorods, while also providing significant field enhancement between them, as was discussed above. The reshaping of electromagnetic fields in plasmonic nanorod-based metamaterials results in a strong and tuneable effective bulk nonlinear response, which can be engineered by changing the structural parameters of the metamaterial from the visible to the NIR spectral ranges.[106] Strong SHG enhancement for TM-polarized fundamental light was observed in the ENZ spectral region (**Figure 5a**).

Additionally, the strong nonlinear response either to TM- or TE- polarized fundamental light can be engineered through designing Fabry–Pérot resonances or guided modes of the metamaterial slab.[107] Generally, SHG from the nanostructures can be enhanced by implementing a 'double-resonance' condition, with plasmonic enhancement at both fundamental and SHG wavelengths.[102,103] It can be easily done with a metamaterial where both the incident light and the generated SHG waves are resonantly coupled to the metamaterial-guided modes.[107] The estimated value of an effective second-order susceptibility for the nanorod metamaterial of $\chi^{(2)} \sim 10^{-6}$ ESU is comparable to that of common nonlinear optical crystals.[106,107] Similarly, nickel nanorod metamaterials have been employed to demonstrate plasmonic enhancement of both linear and nonlinear magneto-optical responses.[52] SHG emission in nanorod metamaterials can also be used for tracking the location of nanoparticles placed inside them.[108]

6.2. Third-Order Nonlinear Effects

The other source of optical nonlinearity in metals is related to optically-induced change in the energy distribution of the free-electron gas in the conduction band, leading to the alteration of the metal optical properties and thus to Kerr-type nonlinearity, including nonlinear refraction and nonlinear absorption.[109] Upon absorption of an illuminating ultra-short laser pulse through interband and/or intraband (phonon- and geometry-assisted) transitions, high-energy 'hot' electrons are excited in the conduction band (Figure 5b), which reach a thermal equilibrium among themselves at a 100-fs time scale upon electron-electron scattering.[110] Before the excited hot electrons re-establish their thermal distribution with the lattice temperature at a timescale of a few picoseconds upon electron-phonon scattering, the permittivity of the metal and, therefore, the optical properties of the metamaterial are changed. This Kerr-type effect is usually weak, but it can be enhanced in configurations sensitive to the permittivity changes and/or providing field enhancement effects, both of which happen in plasmonic nanorod metamaterials. Pump-probe experiments showed ∼ 70% modulation of light transmission through the nanorod metamaterial following femtosecond pulse illumination[25] (Figure 5c). The metamaterial nonlinearity describing this effect is extremely large, as the metamaterial thickness is only a few hundred nm. The ultrafast response confirms the electron gas heating as the underlying mechanism. The strongest nonlinearity was observed at the position of the coupled nanorod transverse resonance (short-wavelength peak) and in the ENZ spectral range, where nonlocal effects are important (long-wavelength peak). The large optical transmission modulation was related to the electron-temperature-dependent hybridization of the extraordinary wave in the metamaterial with the additional electromagnetic wave supported due to the nonlocality discussed above. Such hybridization can be greatly enhanced by the reduction of the losses by annealing the sample[66] and/or by decreasing the operational temperature.[111]

Quantitative analysis of the Kerr-nonlinearity of the metamaterials using a z-scan technique subsequently gave the nonlinear refraction coefficient $\gamma \approx -2.4 \times 10^{-11}$ cm^2 W^{-1} and nonlinear absorption coefficient $\beta \approx -9967$ cm GW^{-1}[112] near the ENZ
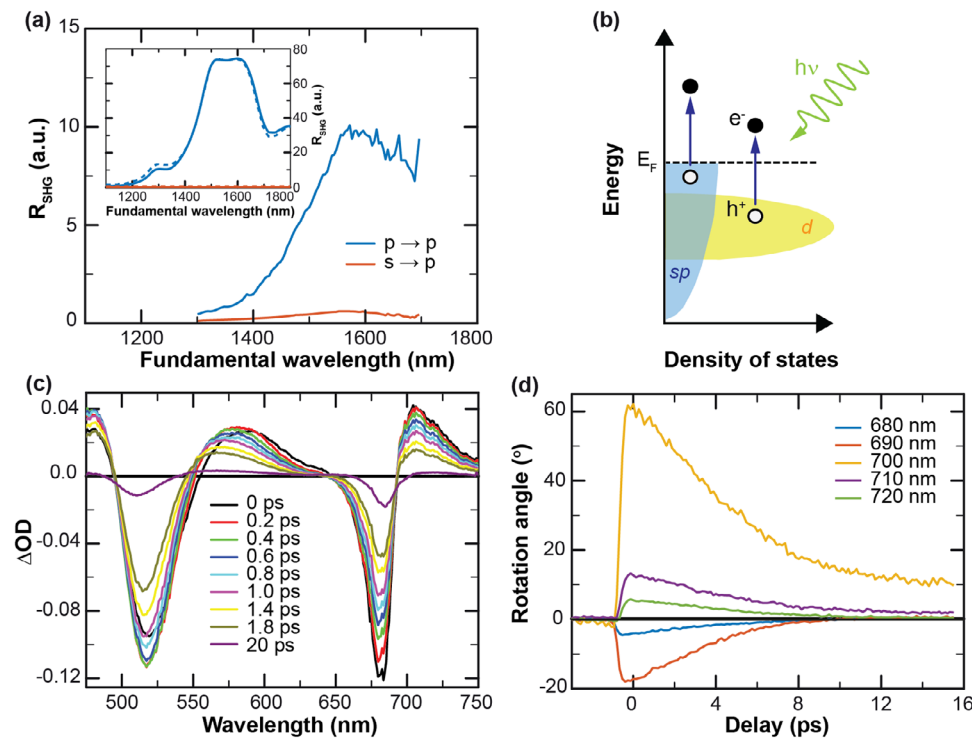
Figure 5. a) SHG signal from a nanorod metamaterial measured in reflection for s- (TE) and p- (TM) polarized illumination at 45°. The inset shows full-wave numerical modeling of the SHG intensity based on the hydrodynamic model. Reproduced with permission.[106] Copyright 2018, Optica Publishing Group. b) Schematics showing interband and intraband absorption mechanisms of the modification of gold permittivity. c) Light-induced change in the optical density of the nanorod metamaterial at various times after a femtosecond pump pulse. Reproduced with permission.[25] Copyright 2011, Macmillan Publishers Limited. d) A change in a rotation angle of the probe polarization ellipse as a function of the delay between the probe and pump pulses for various probe wavelengths. Reproduced with permission.[26] Copyright 2017, Macmillan Publishers Limited.

wavelength. Compared to those measured at the same wavelength for a smooth Au film, $|\gamma|$ and $|\beta|$ of the nanorod metamaterial are approximately 20 and 100 times larger, respectively. The nonlinear coefficients of the metamaterial can have both positive and negative values, corresponding to optically induced focusing or defocusing, and to induced absorption or transparency, which can be pre-engineered at the metamaterial fabrication stage via the design of the ENZ spectral position. Both transient relaxation time and magnitude of the nonlinear response depend on the spatial profile of the induced electron temperature, also defined by the metamaterial geometry.[113]

Using strong anisotropy and high nonlinearity of the nanorod metamaterials, ultrafast modulation of the polarization state of the transmitted light can be achieved via dissimilar modulation of propagation characteristics for TE- and TM-polarized modes. Strong changes in the orientation of the polarization of the probe beam up to 60° in the ENZ regime accompanied by its elliptization have been demonstrated[26,114] (Figure 5d). Modulation of light in integrated geometries by introducing the metamaterial on the top of Si waveguides has also been shown.[115]

7. Spontaneous Emission and Energy Transfer

7.1. Spontaneous Emission Enhancement

The process of spontaneous emission is strongly affected by the electromagnetic environment in which the emitters are located,

which is known as the Purcell effect.[116] Particularly, the spontaneous emission rate $\Gamma(\omega)$ is directly proportional to the local density of optical states (LDOS), $\rho(\omega, r)$, available for the radiation of the excited emitters:

$$\Gamma(\omega) \propto \rho(\omega, r) \tag{4}$$

In this respect, the possibility of controlling spontaneous emission by engineering the LDOS via the design of individual nanostructures and nanostructured materials has been widely used. Hyperbolic metamaterials have been shown to constitute an interesting alternative to single resonant nanostructures in order to achieve non-resonant broadband spontaneous emission enhancement.[117,118] Due to their extended isofrequency surfaces, as discussed in Section 3, hyperbolic metamaterials support unique high-wavevector propagating modes, evanescent in conventional media, which leads to larger LDOS than that in materials having isotropic or elliptic dispersion and ultimately makes them perfect candidates for the control of spontaneous emission over a large bandwidth. Related to the metamaterial LDOS is also a giant self-torque experienced by the emitter inside a hyperbolic metamaterial in order to minimize its energy in its own local radiation field.[119] More generally, the LDOS and the related local-field distribution also make an important contribution to the conventional optomechanical forces acting on an object placed inside the metamaterial.[120]
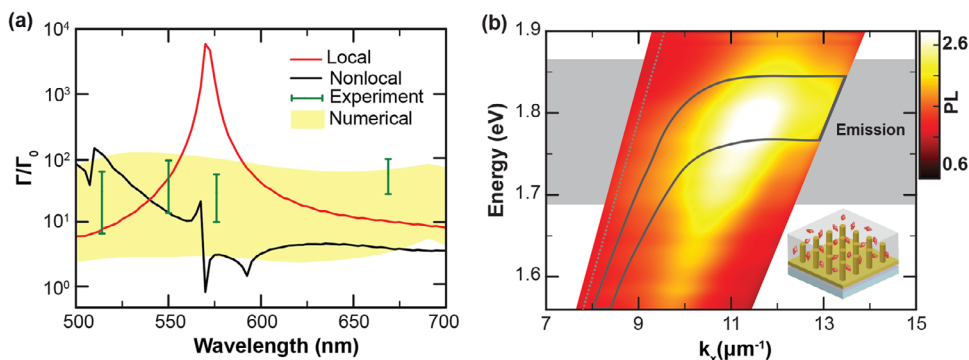
Figure 6. a) Spectral dependence of the spontaneous emission rate enhancement in side a plasmonic nanorod metamaterial averaged over the dipole orientations, obtained from (red) local EMT, (black) nonlocal EMT, (bars) experimental data obtained by applying the inverse Laplace transform to the measured decay curves. Shaded area corresponds to the width of the simulated lifetime distribution after averaging over the dipole position within the elementary cell of the metamaterial. Reproduced with permission.[67] Copyright 2017, Springer Nature. b) Experimental dispersion of photoluminescence (PL) enhancement measured for TM-polarized emission from dye-functionalized metamaterial layer. The position of the TM mode is marked with black lines as a guide to the eye. The light line in air (gray dotted line) and the emission band of the dye (grey-shaded region) are also shown. Inset: schematics of a nanorod metamaterial doped with dye molecules. Reproduced with permission.[24] Copyright 2017, American Chemical Society.

The first experimental investigations of the enhancement of spontaneous emission with hyperbolic metamaterials were performed using emitters deposited on top of a silver nanorod-based metamaterial[117] and a metallo-dielectric multilayers,[121] both exhibiting hyperbolic dispersion. Time-resolved photoluminescence measurements, however, showed only a small reduction of the lifetime of the emitters. Further investigations have however revealed higher enhancements of the decay rates for emitters placed inside the hyperbolic metamaterial, where the high-wavevector states are more easily accessible.[122,123]

7.1.1. Influence of Nonlocality on Spontaneous Emission in Nanorod Metamaterials

As discussed in Section 3, plasmonic hyperbolic nanorod-based metamaterials can exhibit a highly nonlocal electromagnetic response.[67] Although the nonlocal effects have been shown to modify the linear transmission and reflection of the metamaterial only near the ENZ region and in the case of small losses, their influence on the emission processes has been proven to be significant. Nonlocality, resulting in the presence of an additional propagating mode in the material, fundamentally alters the LDOS in both the elliptic and hyperbolic regimes of dispersion and leads to a decrease of the LDOS compared to the one estimated using the local EMT, espcially in the ENZ regime, therefore setting a fundamental limit on the overall emission rate enhancement.

Experimental investigations of the spontaneous emission process inside a nonlocal nanorod-based metamaterial revealed almost wavelength-independent decay rate enhancement across the elliptic, ENZ and hyperbolic regimes of dispersion (**Figure 6a**).[67] This is in strong contrast with decay rate calculations based on the local EMT, predicting extremely strong enhancement of the decay rate near the ENZ wavelength, but in good agreement with the predicted wavelength dependence of the decay rate given by the nonlocal EMT. The remaining differences beetween the theoretical and experimental results stem from the strong dependence of the LDOS on the position of

the emitter within the unit cell, which is not taken into account in the EMT-based calculation methods. Numerical modeling of dipole emission within the exact nanorod metamaterial geometry confirmed the above dependence and is in agreement with both the experimental data and the nonlocal EMT. The experimentally measured distribution of the decay rate enhancement in the range from 10 to 100, therefore, is attributed to various positions of the molecules deposited inside the metamaterial.

Since the emission process is dominated not only by the topology of the metamaterial dispersion given by the local EMT, but mainly nonlocal effects, metamaterials with different geometric parameters but the same local effective medium properties exhibit different Purcell factors. This allows further engineering of spontaneous emission processes by scaling the unit cell of the metamaterial, keeping the properties of the metamaterial calculated using the local EMT the same, but controlling its geometry-dependent LDOS.[67]

7.1.2. Spontaneous Emission Inside Structured Nanorod Metamaterials

Another degree of freedom for the control of the spontaneous emission properties of emitters located inside hyperbolic plasmonic metamaterials can be achieved by structuring of the metamaterial in order to achieve resonant effects as discussed in Section 4. Most of the experimental and theoretical studies are predominantly limited to essentially bulk metamaterials, so that the effects related to waveguided or cavity modes are either not present or suppressed. However, metamaterials of finite sizes, such as waveguides, photonic-crystal-like structures, or resonators, support a complex hierarchy of electromagnetic modes, which play an important role in the spontaneous emission process.[124] In the case of emission into resonant modes of the structured metamaterials, the decay rate and the emission intensity can be greatly enhanced. This was further demonstrated in the case of emitters located inside a hyperbolic nanorod metamaterial slab, showing an enhancement of the fluorescence due

**ADVANCED
SCIENCE NEWS**

www.advancedsciencenews.com

**LASER
& PHOTONICS
REVIEWS**

www.lpr-journal.org

to coupling of the emission to the waveguided plasmon-polariton modes of the slab (Figure 6b).[24] An almost 50-fold reduction of the lifetime of the emitters inside the metamaterial waveguide was observed, whereas a much smaller reduction is achievable for emitters placed on top of the metamaterial, highlighting the strong dependence of the decay rates on the position of the emitters with regard to the metamaterial. The decay dynamics of a theoretically forbidden singlet–triplet transition in a long lifetime phosphorescent ruthenium-based complex (Ru(dpp)) was enhanced by more than 2500 times inside the hyperbolic nanorod metamaterial, which is attributed to the interplay between the local density of optical states and strongly inhomogeneous electromagnetic fields inside the metamaterial.[125]

7.2. Förster Resonance Energy Transfer

While engineering the local density of optical states provides an efficient control over the spontaneous emission rate, its influence on the Förster resonance energy transfer (FRET) process has been a topic of an ongoing debate underlined by disparate experimental and theoretical results. Many different structures have been investigated in this context, such as plasmonic films, microcavities, nanoparticles and nanoantennas, as well as multilayer hyperbolic metamaterials.[126] Recently, a nanorod-based hyperbolic metamaterial has also been considered for the control of the FRET process.[127] Donor-acceptor pairs placed inside the gold nanorod-based metamaterial, providing a 12-fold increase in the LDOS, exhibited a 13-fold increase of the FRET rate along with only slight variations in the FRET efficiency compared to those located on glass. This geometry shows great potential for the development of FRET-based applications such as biomedical imaging, organic solar cells and light-emitting sources.

8. Recent Developments

The relatively easy fabrication technique of the nanorod-based metamaterials and the possibility of electrodepositing different materials into the porous AAO matrix has paved the way for the development of novel structures with designed material and optical properties for novel applications, including photocatalysis, enhanced magneto-optics, neuromorphic devices, and many others.

The reactive tunnel junctions based on electrically driven plasmonic nanorod metamaterials described in Section 5.2 have been shown to be not only top-performing sensors but also efficient nanoreactors allowing controllable activation of chemical reactions at the nanoscale. These nanoreactors take advantage of the generation of hot electrons in the gold nanorod tips, via elastic tunneling of electrons, and can provide real-time monitoring of chemical transformation of molecules introduced into the junctions, by observing the changes in the light emission from the metamaterial generated by the inelastic tunneling.[92]

Electrical and optical memory effects in the metamaterial-supported tunnel junctions emulating synaptic behavior have also been recently investigated. Particularly, simultaneous multilevel switching of the resistance and the light emission of the junctions was demonstrated, upon non-volatile programming of the tunnel junctions, achieved via hot-electron-mediated

chemical reactions controlled by the chemical environment.[128] Tunneling-based metamaterial designs also provide an opportunity for the realization of nanoscale, electrically-driven incoherent light sources, tuneable by engineering the emission spectrum defined by the metamaterial modes.[95] Such sources, due to a small capacitance of nanorod tunnel junctions, may support very high modulation rates. Broadband LDOS enhancement provided by nanorod hyperbolic metamaterials[117] has been used to realize metamaterial-assisted lasing (**Figure 7**a).[129]

In addition, new anisotropic metamaterial designs, such as arrays of plasmonic nanotubes, coaxial structures and nanocones, derived from the nanorod-based geometry, have also been recently developed. Nanotube- and coaxial-based structures have been shown to provide access to a wider range of plasmonic modes, enhancing their capabilities in terms of tuneability of their optical properties and operation at normal incidence.[132–134] The latter is a crucial advantage since most interesting functionalities described above require oblique illumination of the nanorod-based metamaterial with the electric field of the incident wave having a component along the nanorods. In this respect, highly tuneable, angular independent absorption of light in nanotube plasmonic arrays has been demonstrated to be useful for the design of sensors and colour filters.[135] Such metamaterials also exhibit an improved surface area, beneficial for biosensing and catalysis applications. Derived architectures of nanorod metamaterials made by electrodeposition of metal catalysts, such as copper, have also become of increased interest to drive and improve the efficiency of photocatalytic processes, in particular for the reduction of carbon dioxide.[51] Functionalization of the nanorod metamaterial with TiO_2 also leads to photocatalytic activity,[136] while deposition of platinum nanoparticles has been used to achieve water-splitting for green-energy hydrogen production (Figure 7b).[130] Besides nanotube-based structures, transition metamaterials[75] based on arrays of nanocones have been recently developed. These gradient-index metamaterials are fabricated using a scalable method utilizing ion-etching of electrochemically grown nanorods. Arrays of closely packed cones with ultrasharp apexes of $\lesssim$ 2 nm were achieved to provide strongly coupled plasmonic modes together with an extremely high density of electromagnetic hot spots, useful for surface-enhanced Raman spectroscopy, which has already been demonstrated for the case of the nanorod metamaterial,[137] as well as hot-carrier plasmonics and photocatalysis.[62] Finally, using the same electrodeposition technique, a layered nanorod metamaterial has been realized. Particularly, a nanometer-thin zinc oxide layer has been introduced inside each rod at a variable height.[53] Under resonant excitation, these gaps produce high localization and enhancement of the field, which results in an array of hot spots and can be used in a variety of applications including nonlinear and memristive devices. Alternatively, nanometer-thin gaps in the nanorod metamaterials can be fabricated using chemical functionalization.[138] Metamaterial-assisted near-field heat transfer beyond the classic blackbody radiation limit has been demonstrated with the use of silicon nanorod metamaterials.[61] Magneto-optical metamaterials exhibiting an enhanced Faraday effect and nonreciprocal transmission have been demonstrated introducing magnetic material (Ni) in the plasmonic (Au) metamaterial structure.[139] Arrays of metallic nanohelixes have shown very large circular dichroism and have been used for the
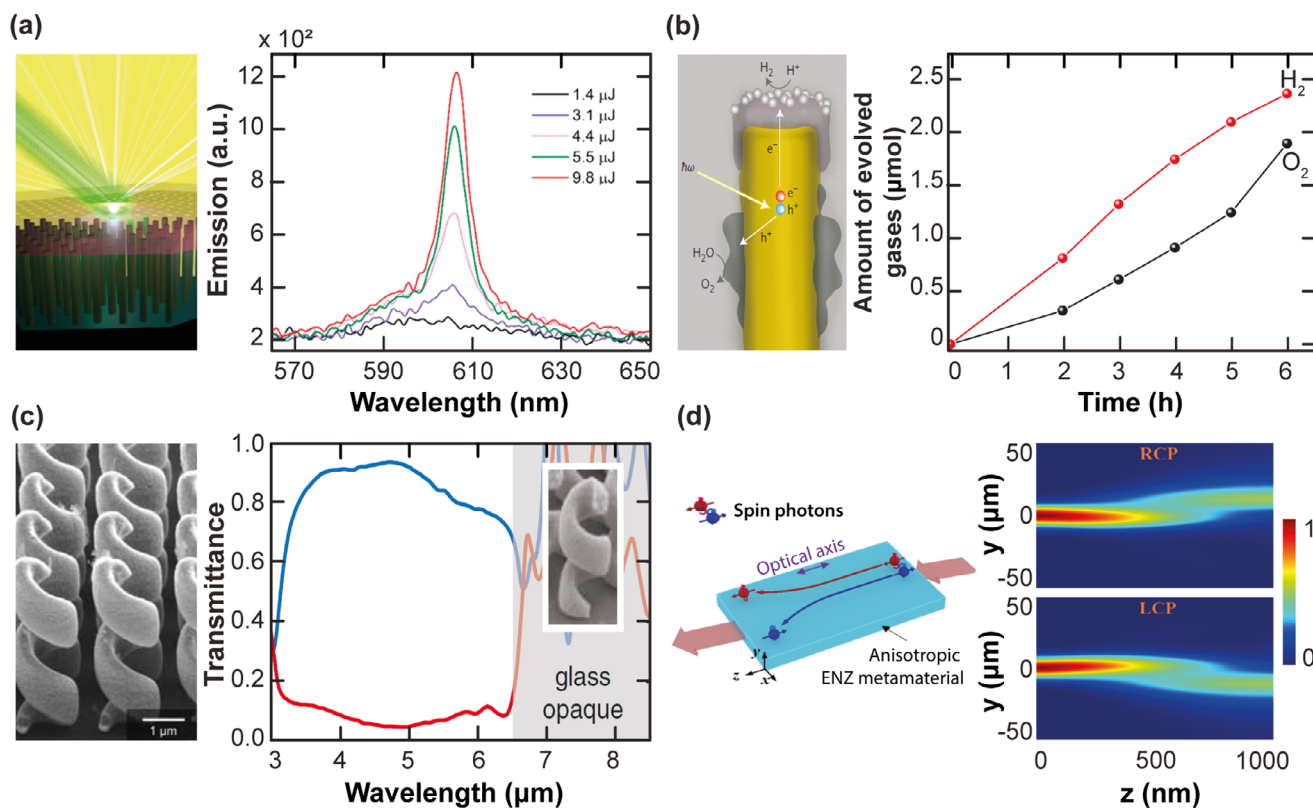
Figure 7. a) Schematics of a nanorod hyperbolic metamaterial functionalized with Rhodamine 101 dye and its emission spectra for various pump powers. Reproduced with permission.[129] Copyright 2017, American Chemical Society. b) Water-splitting and production of H_2 using a gold nanorod metamaterial functionalized with platinum nanoparticles. Reproduced with permission.[130] Copyright 2013, Macmillan Publishers Limited. c) SEM image of an array of gold nanohelixes (the scale bar is 1 µm) and its transmittance for left- (red) and right- (blue) circularly polarized light. Reproduced with permission.[131] Copyright 2009, Association for the Advancement of Science. c) Numerical simulations of the photonic Hall effect using an Ag nanorod metamaterial. Reproduced with permission.[131] Copyright 2021, Optical Society of America.

realization of broadband circular polarisers (Figure 7c),[131,140] chirality-assisted detection of hydrogen,[141] and for the studies of chiroptical modes.[142] Giant anisotropy of the plasmonic nanorod metamaterial has been proposed as a means for the realization of the photonic spin Hall effect (Figure 7d).[143] Metamaterial-assisted image reproduction beyond Abbe's diffraction limit has been experimentally demonstrated using near-field optical microscopy.[144] Recent developments in the area of structured light have also highlighted the potential of nanorod-based metamaterials and their strong anisotropy and nonlocality for the manipulation of polarization properties and spin-orbit coupling in vector vortex beams, useful in a variety of applications, including high-resolution imaging.[145,146]

9. Outlook

We have presented an overview of linear and nonlinear optical properties of plasmonic nanorod metamaterials and their main application areas in nanophotonics. Particular attention was given to the theoretical description of the metamaterials, which is of paramount importance for the efficient design and optimization of their optical mode structure for bespoke applications. Their nonlocal behavior, in particular, has been shown to play a crucial role in nonlinear and quantum optical processes,

for instance, by setting a fundamental limit on the possible emission rate enhancement. The benefits of additional nanostructuring for the engineering of the modes of the metamaterial system in order to achieve waveguides and photonic crystals with unusual properties have been explained. Nonlinearities in nanorod-based metamaterials have also been discussed, highlighting their potential for tailoring second harmonic generation, as well as an enhanced Kerr-type optical response, useful for the design of ultrafast all-optical switching devices, including those capable of polarization control. Engineered epsilon-near-zero response, where the nonlinear modulation of the refractive index is strongly enhanced, may be useful for development of time-varying media. Nanorod-based metamaterials have also been shown to provide a highly attractive platform for the engineering of spontaneous emission and Förster energy transfer, allowing broadband non-resonant enhancement of the emission and energy transfer rates, important for intergrated quantum photonic sources. A unique potential of the nanorod-based metamaterials for a large variety of sensing applications was demonstrated, taking advantage of the extremely high sensitivity of the metamaterial optical response to the changes in the refractive index in the surroundings of the nanorods. Strong, optically controlled anisotropy of the metamaterials opens a playground for the manipulation of vectorial modes of light. Thanks to the high tuneability of such

metamaterials in terms of their material constituents and geometrical properties together with the constant improvement of fabrication techniques, the development of novel structures derived from nanorod-based metamaterials, such as nanocones, nanotubes, coaxial, and nanogap arrays, offering novel or enhanced optical effects, has recently gained a lot of interest. Additional incorporation of functional materials in this metamaterial platform paves the way toward exciting new applications of nanorod plasmonic metamaterials in hot-electron-driven chemistry, photocatalysis and enhanced sensing.

Acknowledgements

Conflict of Interest

The authors declare no conflict of interest.

Keywords

[1] V. G. Veselago, *Soviet Physics Uspekhi* **1968**, *10*, 509.
[2] D. R. Smith, W. J. Padilla, D. Vier, S. C. Nemat-Nasser, S. Schultz, *Phys. Rev. Lett.* **2000**, *84*, 4184.
[3] R. A. Shelby, D. R. Smith, S. Schultz, *Science* **2001**, *292*, 77.
[4] N. Fang, H. Lee, C. Sun, X. Zhang, *Science* **2005**, *308*, 534.
[5] Z. Liu, H. Lee, Y. Xiong, C. Sun, X. Zhang, *Science* **2007**, *315*, 1686.
[6] D. Schurig, J. Mock, B. Justice, S. A. Cummer, J. B. Pendry, A. Starr, D. Smith, *Science* **2006**, *314*, 977.
[7] N. I. Landy, S. Sajuyigbe, J. J. Mock, D. R. Smith, W. J. Padilla, *Phys. Rev. Lett.* **2008**, *100*, 207402.
[8] P. Wang, A. Krasavin, V. L. Liu, Y. Jiang, Z. Li, X. Guo, L. Tong, A. V. Zayats, *Chem. Rev.* **2022**, *122*, 15031.
[9] V. M. Shalaev, W. Cai, U. K. Chettiar, H.-K. Yuan, A. K. Sarychev, V. P. Drachev, A. V. Kildishev, *Opt. Lett.* **2005**, *30*, 3356.
[10] W. Cai, U. K. Chettiar, A. V. Kildishev, V. M. Shalaev, *Nat. Photonics* **2007**, *1*, 224.
[11] C. M. Soukoulis, S. Linden, M. Wegener, *Science* **2007**, *315*, 47.
[12] J. Yao, Z. Liu, Y. Liu, Y. Wang, C. Sun, G. Bartal, A. M. Stacy, X. Zhang, *Science* **2008**, *321*, 930.
[13] Z. Jacob, L. V. Alekseyev, E. Narimanov, *Opt. Express* **2006**, *14*, 8247.
[14] D. Lu, Z. Liu, *Nat. Commun.* **2012**, *3*, 1205.
[15] D. Lu, J. J. Kan, E. E. Fullerton, Z. Liu, *Nat. Nanotechnol.* **2014**, *9*, 48.
[16] P. Wang, A. V. Krasavin, F. N. Viscomi, A. M. Adawi, J.-S. G. Bouillard, L. Zhang, D. J. Roth, L. Tong, A. V. Zayats, *Laser Photonics Rev.* **2018**, *12*, 1800179.
[17] P. Evans, W. Hendren, R. Atkinson, G. Wurtz, W. Dickson, A. Zayats, R. Pollard, *Nanotechnology* **2006**, *17*, 5746.
[18] A. Poddubny, I. Iorsh, P. Belov, Y. Kivshar, *Nat. Photonics* **2013**, *7*, 948.
[19] N. Maccaferri, Y. Zhao, T. Isoniemi, M. Iarossi, A. Parracino, G. Strangi, F. De Angelis, *Nano Lett.* **2019**, *19*, 1851.
[20] J. Kuttruff, A. Gabbani, G. Petrucci, Y. Zhao, M. Iarossi, E. Pedrueza-Villalmanzo, A. Dmitriev, A. Parracino, G. Strangi, F. De Angelis, D. Brida, F. Pineider, N. Maccaferri, *Phys. Rev. Lett.* **2021**, *127*, 217402.
[21] Y. Zhao, A. Hubarevich, M. Iarossi, T. Borzda, F. Tantussi, J.-A. Huang, F. De Angelis, *Adv. Opt. Mater.* **2021**, *9*, 2100888.
[22] C. Cortes, W. Newman, S. Molesky, Z. Jacob, *J. Opt.* **2012**, *14*, 063001.
[23] A. Kabashin, P. Evans, S. Pastkovsky, W. Hendren, G. Wurtz, R. Atkinson, R. Pollard, V. Podolskiy, A. Zayats, *Nat. Mater.* **2009**, *8*, 867.
[24] D. J. Roth, A. V. Krasavin, A. Wade, W. Dickson, A. Murphy, S. Kéna-Cohen, R. Pollard, G. A. Wurtz, D. Richards, S. A. Maier, A. V. Zayats, *ACS Photonics* **2017**, *4*, 2513.
[25] G. A. Wurtz, R. Pollard, W. Hendren, G. Wiederrecht, D. Gosztola, V. Podolskiy, A. V. Zayats, *Nat. Nanotechnol.* **2011**, *6*, 107.
[26] L. H. Nicholls, F. J. Rodríguez-Fortuño, M. E. Nasir, R. M. Córdova-Castro, N. Olivier, G. A. Wurtz, A. V. Zayats, *Nat. Photonics* **2017**, *11*, 628.
[27] P. V. Kapitanova, P. Ginzburg, F. J. Rodríguez-Fortuño, D. S. Filonov, P. M. Voroshilov, P. A. Belov, A. N. Poddubny, Y. S. Kivshar, G. A. Wurtz, A. V. Zayats, *Nat. Commun.* **2014**, *5*, 3226.
[28] R. M. Córdova-Castro, M. Casavola, M. Van Schilfgaarde, A. V. Krasavin, M. A. Green, D. Richards, A. V. Zayats, *ACS Nano* **2019**, *13*, 6550.
[29] K. Korzeb, M. Gajc, D. A. Pawlak, *Opt. Express* **2015**, *23*, 25406.
[30] Q. Zhang, G. Hu, W. Ma, P. Li, A. Krasnok, R. Hillenbrand, A. Alù, C.-W. Qiu, *Nature* **2021**, *597*, 187.
[31] D. Lee, S. So, G. Hu, M. Kim, T. Badloe, H. Cho, J. Kim, H. Kim, C.-W. Qiu, J. Rho, *ELight* **2022**, *2*, 1.
[32] T. Low, A. Chaves, J. D. Caldwell, A. Kumar, N. X. Fang, P. Avouris, T. F. Heinz, F. Guinea, L. Martin-Moreno, F. Koppens, *Nat. Mater.* **2017**, *16*, 182.
[33] A. Nemilentsau, T. Low, G. Hanson, *Phys. Rev. Lett.* **2016**, *116*, 066804.
[34] C. Wang, S. Huang, Q. Xing, Y. Xie, C. Song, F. Wang, H. Yan, *Nat. Commun.* **2020**, *11*, 1158.
[35] P. Li, M. Lewin, A. V. Kretinin, J. D. Caldwell, K. S. Novoselov, T. Taniguchi, K. Watanabe, F. Gaussmann, T. Taubner, *Nat. Commun.* **2015**, *6*, 7507.
[36] Z. Jacob, *Nat. Mater.* **2014**, *13*, 1081.
[37] G. Hu, J. Shen, C.-W. Qiu, A. Alù, S. Dai, *Adv. Opt. Mater.* **2020**, *8*, 1901393.
[38] W. Ma, P. Alonso-González, S. Li, A. Y. Nikitin, J. Yuan, J. Martín-Sánchez, J. Taboada-Gutiérrez, I. Amenabar, P. Li, S. Vélez, C. Tollan, Z. Dai, Y. Zhang, S. Sriram, K. Kalantar-Zadeh, S.-T. Lee, R. Hillenbrand, Q. Bao, *Nature* **2018**, *562*, 557.
[39] M. Z. Alam, I. De Leon, R. W. Boyd, *Science* **2016**, *352*, 795.
[40] L. Caspani, R. Kaipurath, M. Clerici, M. Ferrera, T. Roger, J. Kim, N. Kinsey, M. Pietrzyk, A. Di Falco, V. M. Shalaev, A. Boltasseva, D. Faccio, *Phys. Rev. Lett.* **2016**, *116*, 233901.
[41] H. W. Lee, G. Papadakis, S. P. Burgos, K. Chander, A. Kriesch, R. Pala, U. Peschel, H. A. Atwater, *Nano Lett.* **2014**, *14*, 6463.
[42] Y.-W. Huang, H. W. H. Lee, R. Sokhoyan, R. A. Pala, K. Thyagarajan, S. Han, D. P. Tsai, H. A. Atwater, *Nano Lett.* **2016**, *16*, 5319.
[43] A. Krasavin, A. Zayats, *Phys. Rev. Lett.* **2012**, *109*, 053901.
[44] T. J. Cui, S. Zhang, A. Alu, M. Wegener, J. Pendry, J. Luo, Y. Lai, Z. Wang, X. Lin, H. Chen, P. Chen, R.-X. Wu, Y. Yin, P. Zhao, H. Chen, Y. Li, Z. Zhou, N. Engheta, V. S. Asadchy, C. Simovski, S. A. Tretyakov, B. Yang, S. D. Campbell, Y. Hao, D. H. Werner, S. Sun, L. Zhou, S. Xu, H.-B. Sun, Z. Zhou, et al., *J. Phys. Photonics* **2024**, https://doi.org/10.1088/2515-7647/ad1a3b.

2300886 (14 of 17)

**ADVANCED
SCIENCE NEWS**

www.advancedsciencenews.com

**LASER
& PHOTONICS
REVIEWS**

www.lpr-journal.org

[45] Z. Fusco, M. Taheri, R. Bo, T. Tran-Phu, H. Chen, X. Guo, Y. Zhu, T. Tsuzuki, T. P. White, A. Tricoli, *Nano Lett.* **2020**, *20*, 3970.

[46] I. Liberal, N. Engheta, *Nat. Photonics* **2017**, *11*, 149.

[47] M. Sander, L. Tan, *Adv. Func. Mater.* **2003**, *13*, 393.

[48] C. Martin, *Science* **1994**, *266*, 1961.

[49] J. Yao, K.-T. Tsai, Y. Wang, Z. Liu, G. Bartal, Y.-L. Wang, X. Zhang, *Opt. Express* **2009**, *17*, 22380.

[50] R. Zang, H. Hu, X. Li, J. Gao, L. Liang, H. Zhang, F. Zhuge, J. Luo, H. Cao, *Opt. Lett.* **2019**, *44*, 2970.

[51] A. Zaleska, A. V. Krasavin, A. V. Zayats, W. Dickson, *Mater. Adv.* **2024**, https://doi.org/10.1039/D3MA01129A.

[52] V. L. Krutyanskiy, I. A. Kolmychek, E. A. Gan'shina, T. V. Murzina, P. Evans, R. Pollard, A. A. Stashkevich, G. A. Wurtz, A. V. Zayats, *Phys. Rev. B* **2013**, *87*, 3.

[53] M. E. Nasir, A. V. Krasavin, R. M. Córdova-Castro, C. P. McPolin, J.-S. G. Bouillard, P. Wang, A. V. Zayats, *Adv. Opt. Mater.* **2021**, *9*, 2001467.

[54] J. Huang, X. Wang, X. L. Phuah, P. Lu, Z. Qi, H. Wang, *Mater. Today Nano* **2019**, *8*.

[55] Y.-J. Jen, M.-J. Lin, H.-M. Wu, H.-S. Liao, J.-W. Dai, *Opt. Express* **2013**, *21*, 10259.

[56] Y.-J. Jen, K.-B. Yang, P.-C. Lin, M.-H. Chung, *Sci. Rep.* **2020**, *10*, 1.

[57] P. Li, Y. Li, Z.-K. Zhou, S. Tang, X.-F. Yu, S. Xiao, Z. Wu, Q. Xiao, Y. Zhao, H. Wang, P. K. Chu, *Adv. Mater.* **2016**, *28*, 2511.

[58] Y. Liang, Y. Xie, D. Chen, C. Guo, S. Hou, T. Wen, F. Yang, K. Deng, X. Wu, I. I. Smalyukh, Q. Liu, *Nat. Comm.* **2017**, *8*.

[59] S. Umadevi, X. Feng, T. Hegmann, *Adv. Funct. Mater.* **2013**, *23*, 1393.

[60] M. K. Sahoo, V. S. A. Anand, A. Kumar, *Nanotechnology* **2023**, *34*, 19.

[61] W. Du, J. Yang, S. Zhang, N. Iqbal, Y. Dang, J.-B. Xu, Y. Ma, *Nano Enargy* **2020**, *78*.

[62] R. M. Cordova-Castro, A. Krasavin, V, M. E. Nasir, A. Zayats, V, W. Dickson, *Nanotechnology* **2019**, *30*, 5.

[63] C. Reinhardt, S. Passinger, B. Chichkov, W. Dickson, G. A. Wurtz, P. Evans, R. Pollard, A. V. Zayats, *Appl. Phys. Lett.* **2006**, *89*, 231117.

[64] J. Elser, R. Wangberg, V. A. Podolskiy, E. E. Narimanov, *Appl. Phys. Lett.* **2006**, *89*, 26.

[65] R. Wangberg, J. Elser, E. Narimanov, V. Podolskiy, *J. Opt. Soc. Am. B* **2006**, *23*, 498.

[66] R. J. Pollard, A. Murphy, W. R. Hendren, P. R. Evans, R. Atkinson, G. A. Wurtz, A. V. Zayats, V. A. Podolskiy, *Phys. Rev. Lett.* **2009**, *102*, 12.

[67] P. Ginzburg, D. J. Roth, M. E. Nasir, P. Segovia, A. V. Krasavin, J. Levitt, L. M. Hirvonen, B. Wells, K. Suhling, D. Richards, V. A. Podolskiy, A. V. Zayats, *Light: Sci. Appl.* **2017**, *6*, e16273.

[68] P. Ginzburg, F. R. Fortuño, G. Wurtz, W. Dickson, A. Murphy, F. Morgan, R. Pollard, I. Iorsh, A. Atrashchenko, P. Belov, Y. Kivshar, A. Nevet, G. Ankonina, M. Orenstein, A. Zayats, *Opt. Express* **2013**, *21*, 14907.

[69] L. Ferrari, C. Wu, D. Lepage, X. Zhang, Z. Liu, *Prog. Quantum. Electron.* **2015**, *40*, 1.

[70] V. P. Drachev, V. A. Podolskiy, A. V. Kildishev, *Opt. Express* **2013**, *21*, 15048.

[71] R. Atkinson, W. Hendren, G. Wurtz, W. Dickson, A. Zayats, P. Evans, R. Pollard, *Phys. Rev. B* **2006**, *73*, 23.

[72] M. Nasir, S. Peruch, N. Vasilantonakis, W. Wardley, W. Dickson, G. Wurtz, A. Zayats, *Appl. Phys. Lett.* **2015**, *107*, 121110.

[73] R. Starko-Bowes, J. Atkinson, W. Newman, H. Hu, T. Kallos, G. Palikaras, R. Fedosejevs, S. Pramanik, Z. Jacob, *J. Opt. Soc. Am. B* **2015**, *32*, 2074.

[74] B. M. Wells, A. V. Zayats, V. A. Podolskiy, *Phys. Rev. B* **2014**, *89*, 3.

[75] B. Wells, Z. A. Kudyshev, N. Litchinitser, V. A. Podolskiy, *ACS Photonics* **2017**, *4*, 2470.

[76] M. Silveirinha, *Phys. Rev. E* **2006**, *73*, 2.

[77] H. Hu, X. Lin, J. Zhang, D. Liu, P. Genevet, B. Zhang, Y. Luo, *Laser Photonics Rev.* **2020**, *14*, 10.

[78] T. Stefaniuk, L. H. Nicholls, R. M. Cordova-Castro, M. E. Nasir, A. V. Zayats, *Adv. Mat.* **2022**, *35*, 2107023.

[79] Y. Meng, Y. Chen, L. Lu, Y. Ding, A. Cusano, J. A. Fan, Q. Hu, K. Wang, Z. Xie, Z. Liu, Y. Yang, Q. Liu, M. Gong, Q. Xiao, S. Sun, M. Zhang, X. Yuan, X. Ni, *Light Sci. Appl.* **2021**, *10*, 1.

[80] I. Staude, M. Decker, M. J. Ventura, C. Jagadish, D. N. Neshev, M. Gu, Y. S. Kivshar, *Adv. Mater.* **2013**, *25*, 1260.

[81] Y. Fan, X. Le Roux, A. Korovin, A. Lupu, A. de Lustrac, *ACS Nano* **2017**, *11*, 4599.

[82] N. Vasilantonakis, M. E. Nasir, W. Dickson, G. A. Wurtz, A. V. Zayats, *Laser Photonics Rev.* **2015**, *9*, 345.

[83] K.-T. Tsai, G. A. Wurtz, J.-Y. Chu, T.-Y. Cheng, H.-H. Wang, A. V. Krasavin, J.-H. He, B. M. Wells, V. A. Podolskiy, J.-K. Wang, Y.-L. Wang, A. V. Zayats, *Nano Lett.* **2014**, *14*, 4971.

[84] A. D. Neira, G. A. Wurtz, A. V. Zayats, *Sci. Rep.* **2015**, *5*, 17678.

[85] W. Dickson, S. Beckett, C. McClatchey, A. Murphy, D. O'Connor, G. A. Wurtz, R. Pollard, A. V. Zayats, *Adv. Mater.* **2015**, *27*, 5974.

[86] P. Wang, M. E. Nasir, A. V. Krasavin, W. Dickson, Y. Jiang, A. V. Zayats, *Acc. Chem. Res.* **2019**, *52*, 3018.

[87] N. Vasilantonakis, G. A. Wurtz, V. A. Podolskiy, A. V. Zayats, *Opt. Express* **2015**, *23*, 14329.

[88] R. Yan, T. Wang, X. Yue, H. Wang, Y.-H. Zhang, P. Xu, L. Wang, Y. Wang, J. Zhang, *Photonics Res.* **2022**, *10*, 84.

[89] P. R. Evans, G. A. Wurtz, R. Atkinson, W. Hendren, D. O'Connor, W. Dickson, R. J. Pollard, A. V. Zayats, *J. Phys. Chem. C* **2007**, *111*, 12522.

[90] D. Vestler, I. Shishkin, E. A. Gurvitz, M. E. Nasir, A. Ben-Moshe, A. P. Slobozhanyuk, A. V. Krasavin, T. Levi-Belenkova, A. S. Shalin, P. Ginzburg, G. Markovich, A. V. Zayats, *Opt. Express* **2018**, *26*, 17841.

[91] M. E. Nasir, W. Dickson, G. A. Wurtz, W. P. Wardley, A. V. Zayats, *Adv. Mater.* **2014**, *26*, 3532.

[92] P. Wang, A. V. Krasavin, M. E. Nasir, W. Dickson, A. V. Zayats, *Nat. Nanotechnol.* **2018**, *13*, 159.

[93] V. V. Yakovlev, W. Dickson, A. Murphy, J. McPhillips, R. J. Pollard, V. A. Podolskiy, A. V. Zayats, *Adv. Mater.* **2013**, *25*, 2351.

[94] L. Liu, Y. Xu, J. Zhu, P. Wang, L. Tong, A. V. Krasavin, *Front. Phys.* **2020**, *8*, 251.

[95] A. V. Krasavin, P. Wang, M. E. Nasir, Y. Jiang, A. V. Zayats, *Nanophotonics* **2020**, *9*, 427.

[96] Y. Jiang, A. Krasavin, V, M. E. Nasir, P. Wang, A. V. Zayats, *Opt. Mat. Express* **2022**, *12*, 4574.

[97] S. Tadigadapa, K. Mateti, *Meas. Sci. Technol.* **2009**, *20*, 092001.

[98] A. Schilling, O. Yavaş, J. Bischof, J. Boneberg, P. Leiderer, *Appl. Phys. Lett.* **1996**, *69*, 4159.

[99] W. Dickson, P. Evans, G. Wurtz, W. Hendren, R. Atkinson, R. Pollard, A. Zayats, *J. Microsc.* **2008**, *229*, 415.

[100] W. Cai, A. P. Vasudev, M. L. Brongersma, *Science* **2011**, *333*, 1720.

[101] A. V. Krasavin, P. Ginzburg, A. V. Zayats, *Laser Photonics Rev.* **2018**, *12*, 1700082.

[102] M. Celebrano, X. Wu, M. Baselli, S. Großmann, P. Biagioni, A. Locatelli, C. De Angelis, G. Cerullo, R. Osellame, B. Hecht, L. Duó, F. Ciccacci, M. Finazzi, *Nat. Nanotechnol.* **2015**, *10*, 412.

[103] P. Ginzburg, A. Krasavin, Y. Sonnefraud, A. Murphy, R. J. Pollard, S. A. Maier, A. V. Zayats, *Phys. Rev. B* **2012**, *86*, 085422.

[104] J. Alberti, H. Linnenbank, S. Linden, Y. Grynko, J. Förstner, *Appl. Phys. B: Lasers Opt.* **2016**, *122*, 45.

[105] A. V. Krasavin, P. Ginzburg, G. Wurtz, A. Zayats, *Nat. Commun.* **2016**, *7*, 11497.

[106] B. Wells, A. Y. Bykov, G. Marino, M. E. Nasir, A. V. Zayats, V. A. Podolskiy, *Optica* **2018**, *5*, 1502.

[107] G. Marino, P. Segovia, A. V. Krasavin, P. Ginzburg, N. Olivier, G. A. Wurtz, A. V. Zayats, *Laser Photonics Rev.* **2018**, *12*, 1700189.

[108] P. Segovia, G. Marino, A. V. Krasavin, N. Olivier, G. A. Wurtz, P. A. Belov, P. Ginzburg, A. V. Zayats, *Opt. Express* **2015**, *23*, 30730.

[109] A. Y. Bykov, Y. Xie, A. V. Krasavin, A. V. Zayats, *Nano Lett.* **2023**, *23*, 2786.

[110] A. M. Brown, R. Sundararaman, P. Narang, W. A. Goddard III, H. A. Atwater, *ACS Nano* **2015**, *10*, 957.

[111] J.-S. G. Bouillard, W. Dickson, D. P. O'Connor, G. A. Wurtz, A. V. Zayats, *Nano Lett.* **2012**, *12*, 1561.

[112] A. D. Neira, N. Olivier, M. E. Nasir, W. Dickson, G. A. Wurtz, A. V. Zayats, *Nat. Commun.* **2015**, *6*, 7757.

[113] S. Peruch, A. Neira, G. A. Wurtz, B. Wells, V. A. Podolskiy, A. V. Zayats, *Adv. Opt. Mat.* **2017**, *5*, 1700299.

[114] J. Wu, A. Y. Bykov, A. V. Krasavin, M. E. Nasir, A. V. Zayats, *Appl. Phys. Lett.* **2023**, *123*, 17.

[115] A. D. Neira, G. A. Wurtz, P. Ginzburg, A. V. Zayats, *Opt. Express* **2014**, *22*, 10987.

[116] E. M. Purcell, *Phys. Rev.* **1946**, *69*, 681.

[117] M. Noginov, H. Li, Y. A. Barnakov, D. Dryden, G. Nataraj, G. Zhu, C. Bonner, M. Mayy, Z. Jacob, E. Narimanov, *Opt. Lett.* **2010**, *35*, 1863.

[118] H. N. Krishnamoorthy, Z. Jacob, E. Narimanov, I. Kretzschmar, V. M. Menon, *Science* **2012**, *336*, 205.

[119] P. Ginzburg, A. V. Krasavin, A. N. Poddubny, P. A. Belov, Y. S. Kivshar, A. V. Zayats, *Phys. Rev. Lett.* **2013**, *111*, 036804.

[120] A. A. Bogdanov, A. S. Shalin, P. Ginzburg, *Sci. Rep.* **2015**, *5*, 1.

[121] Z. Jacob, J.-Y. Kim, G. V. Naik, A. Boltasseva, E. E. Narimanov, V. M. Shalaev, *Appl. Phys. B: Lasers Opt.* **2010**, *100*, 215.

[122] T. Tumkur, G. Zhu, P. Black, Y. A. Barnakov, C. Bonner, M. Noginov, *Appl. Phys. Lett.* **2011**, *99*, 151115.

[123] W. D. Newman, C. L. Cortes, Z. Jacob, *J. Opt. Soc. Am. B* **2013**, *30*, 766.

[124] A. P. Slobozhanyuk, P. Ginzburg, D. A. Powell, I. Iorsh, A. S. Shalin, P. Segovia, A. V. Krasavin, G. A. Wurtz, V. A. Podolskiy, P. A. Belov, A. V. Zayats, *Phys. Rev. B* **2015**, *92*, 195127.

[125] D. J. Roth, P. Ginzburg, L. M. Hirvonen, J. A. Levitt, M. E. Nasir, K. Suhling, D. Richards, V. A. Podolskiy, A. V. Zayats, *Laser Photonics Rev.* **2019**, *13*, 1900101.

[126] R. Deshmukh, S.-A. Biehs, E. Khwaja, T. Galfsky, G. S. Agarwal, V. M. Menon, *ACS Photonics* **2018**, *5*, 2737.

[127] D. J. Roth, M. E. Nasir, P. Ginzburg, P. Wang, A. Le Marois, K. Suhling, D. Richards, A. V. Zayats, *ACS Photonics* **2018**, *5*, 4594.

[128] P. Wang, M. E. Nasir, A. V. Krasavin, W. Dickson, A. V. Zayats, *Nano Lett.* **2020**, *20*, 1536.

[129] R. Chandrasekar, Z. Wang, X. Meng, S. I. Azzam, M. Y. Shalaginov, A. Lagutchev, Y. L. Kim, A. Wei, A. V. Kildishev, A. Boltasseva, V. M. Shalaev, *ACS Photonics* **2017**, *4*, 674.

[130] S. Mubeen, J. Lee, N. Singh, S. Kraemer, G. D. Stucky, M. Moskovits, *Nat. Nanotechnol.* **2013**, *8*, 247.

[131] J. K. Gansel, M. Thiel, M. S. Rill, M. Decker, K. Bade, V. Saile, G. von Freymann, S. Linden, M. Wegener, *Science* **2009**, *325*, 1513.

[132] A. Murphy, J. McPhillips, W. Hendren, C. McClatchey, R. Atkinson, G. Wurtz, A. V. Zayats, R. J. Pollard, *Nanotechnology* **2010**, *22*, 045705.

[133] A. Murphy, Y. Sonnefraud, A. Krasavin, P. Ginzburg, F. Morgan, J. McPhillips, G. Wurtz, S. Maier, A. Zayats, R. Pollard, *Appl. Phys. Lett.* **2013**, *102*, 103103.

[134] J. McPhillips, A. Murphy, M. P. Jonsson, W. R. Hendren, R. Atkinson, F. Hook, A. V. Zayats, R. J. Pollard, *ACS Nano* **2010**, *4*, 2210.

[135] F. Lotti, C. L. Westgate, A. Zaleska, W. Dickson, C. D. Burgess, A. V. Zayats, *unpublished*.

[136] C. Li, J. Liu, Z. Wu, Z. Chen, J. Jiang, Z. Dou, X. Liu, M. Fu, D. He, Y. Wang, *Adv. Opt. Mater.* **2021**, *9*, 22.

[137] M. D. Doherty, A. Murphy, R. J. Pollard, P. Dawson, *Phys. Rev. X* **2013**, *3*, 1.

[138] Z.-Q. Cheng, F. Nan, D.-J. Yang, Y.-T. Zhong, L. Ma, Z.-H. Hao, L. Zhou, Q.-Q. Wang, *Nanoscale* **2015**, *7*, 1463.

[139] B. Fan, M. E. Nasir, L. H. Nicholls, A. V. Zayats, V. A. Podolskiy, *Adv. Opt. Mat.* **2019**, *7*, 1801420.

[140] J. Kaschke, L. Blume, L. Wu, M. Thiel, K. Bade, Z. Yang, M. Wegener, *Adv. Opt. Mater.* **2015**, *3*, 1411.

[141] M. Matuschek, D. P. Singh, H.-H. Jeong, M. Nesterov, T. Weiss, P. Fischer, F. Neubrech, N. Liu, *Small* **2018**, *14*, 7.

[142] F. Bai, J. Deng, M. Yang, J. Fu, J. Ng, Z. Huang, *Nanotechnology* **2016**, *27*, 11.

[143] H. Chen, D. Guan, W. Zhu, H. Zheng, J. Yu, Y. Zhong, Z. Chen, *Opt. Lett.* **2021**, *46*, 4092.

[144] B. D. F. Casse, W. T. Lu, Y. J. Huang, E. Gultepe, L. Menon, S. Sridhar, *Appl. Phys. Lett.* **2010**, *96*, 2.

[145] V. Aita, A. V. Zayats, *IEEE Photonics J.* **2022**, *15*, 1.

[146] V. Aita, M. Shevchenko, F. J. Rodríguez-Fortuño, A. V. Zayats, *Phys. Rev. B* **2024**, *109*, 125433.

Diane J. Roth obtained her Diplôme d'Ingénieur (recognized as M.Sc. in Engineering) and M.Sc. degree in Photonics for Nanosciences & Life Sciences, as part of a dual degree program between Télécom Physique Strasbourg and the University of Strasbourg. She then joined King's College London where she attained the degree of Ph.D. in Physics in 2017. Since then, her work has focused on the development of practical applications of metamaterials and metasurfaces, as well as experimental verifications of fundamental optical phenomena in the fields of plasmonics and nanophotonics.

Alexey V. Krasavin received his B.Sc. (with honors) and M.Sc. (with honors) degrees from Moscow Institute of Physics and Technology. In 2006, he was awarded a Ph.D. degree in Physics from the University of Southampton and joined Queen's University Belfast as a Research Fellow. Since 2010 he works at King's College London. His research interests include active manipulation of light at the nanoscale, nonlinear plasmonic-assisted effects, plasmonic-enhanced fluorescence, nonlocal and quantum phenomena.

Anatoly V. Zayats is a chair in experimental physics and head of the Photonics & Nanotechnology at the Department of Physics, King's College London. He is also a co-director of the London Centre for Nanotechnology and London Institute for Advanced Light Technologies. His research interests include nanophotonics and plasmonics, metamaterials and metasurfaces, electromagnetic field topology and optical spin-orbit coupling, and nonlinear and ultrafast optics.